AIP | Applied Physics Reviews

Harnessing large deformation and instabilities of soft dielectrics: Theory, experiment, and application

Xuanhe Zhao and Qiming Wang

Citation: Applied Physics Reviews **1**, 021304 (2014); doi: 10.1063/1.4871696
View online: http://dx.doi.org/10.1063/1.4871696
View Table of Contents: http://scitation.aip.org/content/aip/journal/apr2/1/2?ver=pdfcov
Published by the AIP Publishing

APPLIED PHYSICS REVIEWS

Harnessing large deformation and instabilities of soft dielectrics: Theory, experiment, and application

Xuanhe Zhao[1,2,a)] and Qiming Wang[2]
[1]*Soft Active Materials Laboratory, Department of Mechanical Engineering, Massachusetts Institute of Technology, Cambridge, MA 02139, USA*
[2]*Department of Mechanical Engineering and Materials Science, Duke University, Durham, North Carolina 27708, USA*

(Received 19 February 2014; accepted 1 April 2014; published online 6 May 2014)

Widely used as insulators, capacitors, and transducers in daily life, soft dielectrics based on polymers and polymeric gels play important roles in modern electrified society. Owning to their mechanical compliance, soft dielectrics subject to voltages frequently undergo large deformation and mechanical instabilities. The deformation and instabilities can lead to detrimental failures in some applications of soft dielectrics such as polymer capacitors and insulating gels but can also be rationally harnessed to enable novel functions such as artificial muscle, dynamic surface patterning, and energy harvesting. According to mechanical constraints on soft dielectrics, we classify their deformation and instabilities into three generic modes: (i) thinning and pull-in, (ii) electro-creasing to cratering, and (iii) electro-cavitation. We then provide a systematic understanding of different modes of deformation and instabilities of soft dielectrics by integrating state-of-the-art experimental methods and observations, theoretical models, and applications. Based on the understanding, a systematic set of strategies to prevent or harness the deformation and instabilities of soft dielectrics for diverse applications are discussed. The review is concluded with perspectives on future directions of research in this rapidly evolving field. © *2014 AIP Publishing LLC*. [http://dx.doi.org/10.1063/1.4871696]

TABLE OF CONTENTS

I. INTRODUCTION 1
A. Soft dielectrics. 2
B. Large deformation and instabilities of soft dielectrics. 2
II. ELECTROMECHANICS OF DEFORMABLE DIELECTRICS 3
A. Kinematics and equilibrium conditions 3
B. Constitutive law 5
1. Ideal dielectric model 6
2. Incompressible neo-Hookean model 6
C. Stability against linear perturbation 6
III. SOFT-DIELECTRIC FILMS. 7
IV. THREE GENERIC MODES OF DEFORMATION AND INSTABILITIES. 8
A. Mode I: Thinning and pull-in instability . . . 8
1. Experimental method 9
2. Theoretical analysis 9
B. Mode II: Electro-creasing to cratering instabilities 10
1. Experimental method 10
2. Theoretical analysis 11
C. Mode III: Electro-cavitation instability 12
1. Experimental method 12
2. Theoretical analysis 13
V. SUPPRESSING ELECTROMECHANICAL INSTABILITIES. 13
A. Enhancing actuation strain by suppressing pull-in instability 13
1. Soft dielectrics with stiffening properties to suppress pull-in instability 14
2. Mechanical pre-stretches to delay pull-in instability. 15
B. Enhancing electrical energy density by suppressing all modes of instabilities 16
VI. HARNESSING ELECTROMECHANICAL INSTABILITIES FOR APPLICATIONS 17
A. Harnessing pull-in instability for giant actuation strain 17
B. Harnessing electro-creasing to cratering instability. 17
1. Dynamic surface patterning 18
2. Active control of biofouling 18
VII. FUTURE DIRECTIONS 19
A. Non-ideal dielectric properties of soft dielectrics. 19
B. Viscoelasticity of soft dielectrics 19
C. Fracture and fatigue of soft dielectrics 20
D. Soft-dielectric composites 20
E. Computational models of soft dielectrics . . 20

a)Email: zhaox@mit.edu

I. INTRODUCTION

A. Soft dielectrics

Subjected to voltages, all dielectrics deform. The attainable deformation induced by voltages, however, varies markedly from one type of dielectric to another. Electrostrictive and piezoelectric crystals and ceramics, with moduli of a few gigapascal, can attain strains typically less than 1%.[1–3] The maximum strain of glassy and semicrystalline polymers under voltages is about 10%, as their moduli range from megapascal to gigapascal[4,5] (Fig. 1). These crystals, ceramics, and polymers have been commonly categorized as mechanically stiff dielectrics or, in short, stiff or hard dielectrics.[6–8] The attainable deformation of hard dielectrics under voltages is generally limited by electrical breakdown or fracture of the dielectrics. That is, before a hard dielectric can deform substantially, the applied voltage mobilizes charged species in the dielectric to produce a path of electrical conduction or drive the initiation and propagation of cracks, leading to failure of the dielectric.[9,10]

When glassy and semicrystalline polymers are heated above their glass transition temperatures[11–15] or significantly plasticized by plasticizers,[16] their moduli can be reduced below megapascal. The attainable strains of heated or plasticized polymers under voltages can be enhanced over 10%. With moduli further reduced to a few kilopascal, elastomers and elastomeric gels can be readily deformed over 100% by applied voltages[6,8,17–19] (Fig. 1). These heated or plasticized polymers, elastomers, and elastomeric gels have been categorized as mechanically compliant dielectrics or, in short, compliant or soft dielectrics.[6–8] A distinct feature of soft dielectrics is that they can undergo large deformation and mechanical instabilities subject to voltages before failure.

Recent decades have witnessed unprecedented developments of soft dielectrics in diverse areas and applications. For example, insulating cables and polymer-film capacitors have been made to be more flexible and able to sustain higher voltage and temperature, which requires more compliant and reliable dielectric polymers (Fig. 2(a)). Dielectric gels have been developed to conformally cure around electrical components with complicated geometries for sealing and insulation (Fig. 2(b)). In addition to applications as insulators and capacitors, it has been discovered that applied voltages can actuate dielectric elastomers to strain over 100%[17,20] (Fig. 2(c)). Various types of actuators,[21–33] sensors,[34–36] and energy harvesters[37–45] based on dielectric elastomers have been developed and explored for applications that cannot be fulfilled by traditional transducers. For example, since the actuation strains and stresses of dielectric elastomers can approximate or even exceed those of natural muscles, dielectric elastomers have been regarded as one of the most promising candidates for artificial muscles[8,46] (Fig. 2(c)). As another example, Fig. 2(d) illustrates an energy harvester based on a dielectric elastomer that converts mechanical energy from ocean waves into electrical energy.[39]

B. Large deformation and instabilities of soft dielectrics

At the heart of current research on soft dielectrics is the need to understand and control their large deformation and instabilities under voltages.[47] For soft dielectrics used as insulators and capacitors, it is commonly desirable to restrain their deformation and prevent instabilities in order to enhance reliability and electrical energy densities of the dielectrics.[9,48,49] Conversely, soft-dielectric transducers generally need to be able to achieve large deformation in applications such as artificial muscles and energy harvesters. In addition, while instabilities of soft dielectrics under voltages sometimes lead to failures of the dielectrics, it has been recently discovered that the same instabilities, if rationally controlled, can even give transformative applications and novel functions such as achieving giant actuation strains,[7,50] dynamic surface patterning,[51] and active control of biofouling.[52] Therefore, it is of scientific and technological importance to fundamentally understand and judiciously control large deformation and instabilities of soft dielectrics under various working conditions.

Deformation and instabilities of soft dielectrics involve electromechanical coupling and material and geometrical nonlinearity—a combination of challenging topics in physics and materials science. While existing literatures in the field are generally focused on specific types of soft dielectrics under specific working conditions such as dielectric-elastomer transducers[8,22,27,47,53–56] or insulating cables,[57] a systematic discussion on large deformation and instabilities in various types of soft dielectrics under various working conditions will greatly facilitate the progress of the field, but is still not available.

The current review is targeted at illustrating the fundamental principles that underlie deformation and instabilities

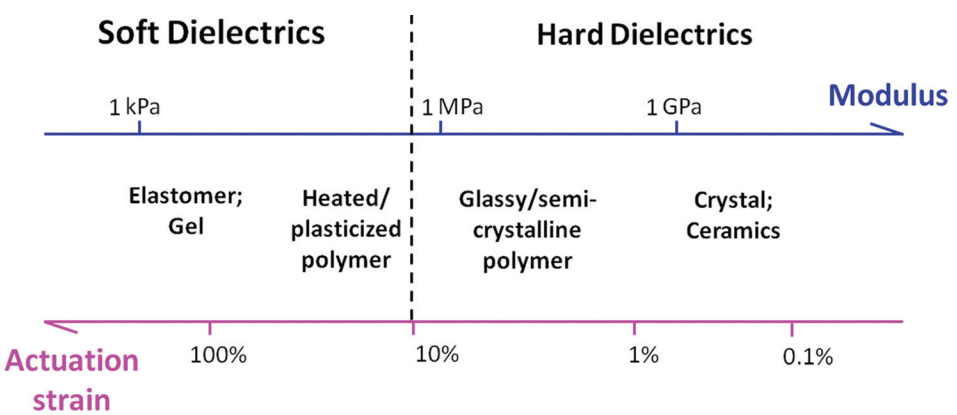

FIG. 1. Classification of dielectrics based on their moduli and actuation strains. The maximum actuation strains of hard dielectrics under voltages are typically less than 10%, while soft dielectrics can achieve actuation strains over 10%.

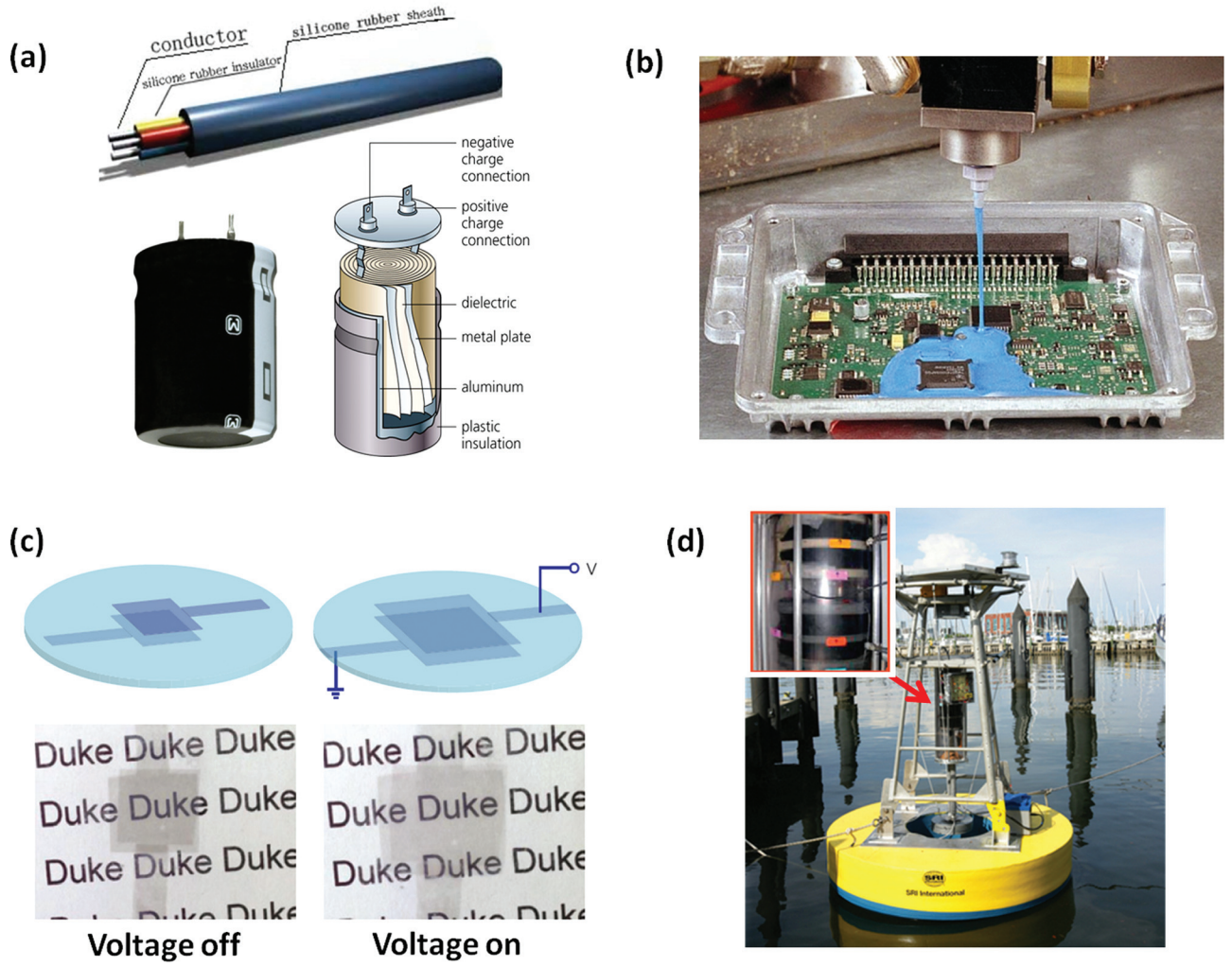

FIG. 2. Examples of applications of soft dielectrics: (a) insulators in insulating cables and polymer-film capacitors, (b) dielectric gels for sealing electronics, (c) artificial-muscle actuators [Reprinted with permission from Zang *et al.*, Nature Mater. **12**, 321–325 (2013). Copyright 2013 Nature Publishing Group[20]], and (d) ocean-wave energy harvesters [Reprinted with permission from Chiba *et al.*, Appl. Energy **104**, 497–502 (2013). Copyright 2013 Elsevier[39]].

of soft dielectrics by integrating state-of-the-art progress in theory, experiments, and applications of this field. We will first summarize the governing equations for electromechanics of deformable dielectrics. Since soft dielectrics mostly appear in the form of films in applications, we will then focus on the deformation and instabilities of soft-dielectric films, which are generally under three types of mechanical constraints: (i) no constraint, (ii) constraint on one surface, and (iii) constraints on both surfaces. According to the mechanical constraints, we will further classify the deformation and instabilities of soft-dielectric films into three generic modes: (i) thinning and pull-in, (ii) electro-creasing to cratering, and (iii) electro-cavitation. Thereafter, we will systematically discuss the strategies to prevent or harness large deformation and instabilities in soft dielectrics and the corresponding applications. The last part of the paper will provide perspectives on future research directions as well as opportunities and challenges in the field.

II. ELECTROMECHANICS OF DEFORMABLE DIELECTRICS

Deformation and instabilities of soft dielectrics under voltages follow the fundamental principles of electromechanics.[58–60] In this section, we will first summarize the physical quantities that characterize soft dielectrics, and the governing equations for their equilibrium and stability conditions. Thereafter, we will discuss constitutive laws for soft dielectrics, especially focusing on the widely used ideal-dielectric model. As soft dielectrics generally undergo large deformation from the reference (undeformed) to current (deformed) configurations, the same physical quantities and governing equations can be expressed in different forms based on the choice of configurations.[61–64] Since different problems of soft dielectrics are more convenient to be solved in different configurations, we will discuss the electromechanics of deformable dielectrics in both reference and current configurations.

A. Kinematics and equilibrium conditions

Consider a dielectric in the reference configuration (Fig. 3(a)). We use the coordinate vector $\mathbf{X}$ of each material particle in the reference configuration to name the material particle. Subjected to electromechanical loads, the dielectric deforms into the current configuration. In the current configuration (Fig.

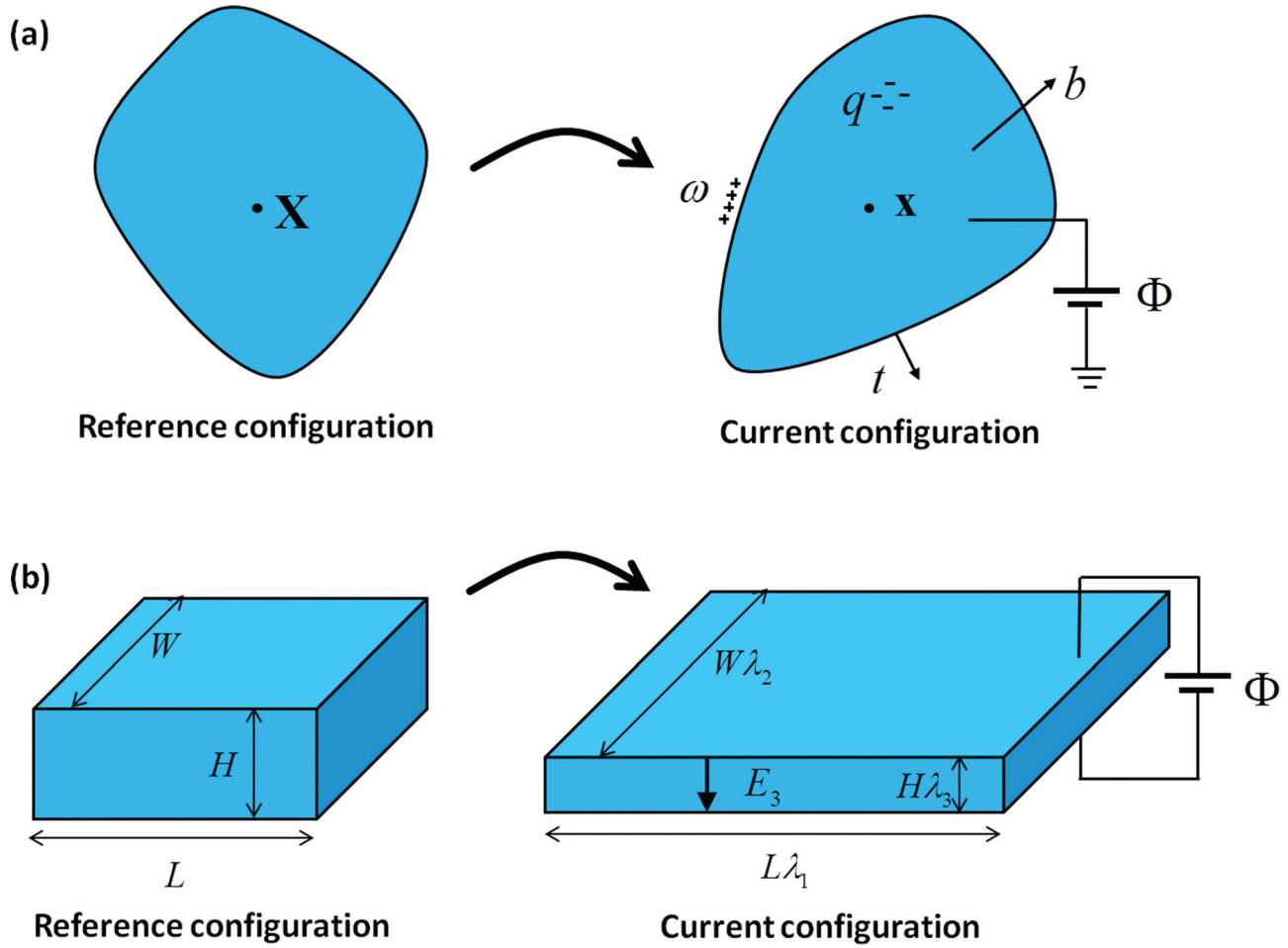

FIG. 3. Schematics of deformation of soft dielectrics: (a) A soft dielectric in the reference (undeformed) configuration and the current (deformed) configuration subjected to electromechanical loads. (b) A soft-dielectric film in the reference and current configurations.

3(a)), a material particle $\mathbf{X}$ occupies a place with coordinate vector $\mathbf{x}$. The deformation gradient tensor is defined by

$$\mathbf{F} = \mathrm{Grad}\mathbf{x}, \tag{1}$$

where Grad is the gradient operator with respect to $\mathbf{X}$. We further denote $\mathrm{d}V$ and $\mathrm{d}v$ as the volume of a material element in the reference and current configurations, respectively. The change in volume due to deformation follows $\mathrm{d}v = J\mathrm{d}V$, where $J = \det \mathbf{F}$. For details of the kinematics of solids, one can refer to, for example, Ogden,[65] Holzapfel,[66] and Gurtin *et al.*[67]

A material particle $\mathbf{X}$ in the dielectric has an electrical potential Φ. The nominal electric field vector is defined, based on the reference configuration, as

$$\tilde{\mathbf{E}} = \mathrm{Grad}\Phi. \tag{2}$$

Correspondingly, the true electric field vector is defined, based on the current configuration, as

$$\mathbf{E} = \mathrm{grad}\Phi, \tag{3}$$

where grad is the gradient operator with respect to $\mathbf{x}$. The nominal and true electric fields are related via $\mathbf{E} = \mathbf{F}^{-T}\tilde{\mathbf{E}}$.

At equilibrium, the Gauss's law and electrical boundary conditions in the reference configuration (i.e., in the Lagrangian form) can be expressed as

$$\mathrm{Div}\tilde{\mathbf{D}} = \tilde{q}, \tag{4a}$$

in the body of the dielectric, and

$$\mathbf{N} \cdot [\tilde{\mathbf{D}}] = \tilde{\omega}, \tag{4b}$$

on the surface of the dielectric. In Eq. (4a), Div is the divergence operator with respect to $\mathbf{X}$, $\tilde{\mathbf{D}}$ is the nominal electric displacement vector defined in the reference configuration, and $\tilde{q}$ is the free charge in a material element divided by the volume of the material element in the reference configuration. In Eq. (4b), $\tilde{\omega}$ is the free charge on a surface element divided by the area of the element in the reference configuration, $\mathbf{N}$ is the unit normal to the surface element in the reference configuration, and the square bracket $[\bullet]$ indicates a discontinuity across the surface.

Equivalently, the Gauss's law and electrical boundary conditions in the current configuration (i.e., in the Eulerian form) give

$$\mathrm{div}\mathbf{D} = q, \tag{5a}$$

in the body of the dielectric, and

$$\mathbf{n} \cdot [\mathbf{D}] = \omega, \tag{5b}$$

on the surface of the dielectric. In Eq. (5a), div is the divergence operator with respect to $\mathbf{x}$, $\mathbf{D}$ is the true electric

displacement vector defined in the reference configuration, and q is the free charge in a material element divided by the volume of the material element in the current configuration (Fig. 3(a)). In Eq. (5b), ω is the free charge on a surface element divided by the area of the element in the current configuration, and $\mathbf{n}$ is the unit normal to the surface element in the current configuration (Fig. 3(a)). In addition, the physical quantities defined in the reference and current configurations in Eqs. (4) and (5) are related via $\mathbf{D} = \mathbf{F}\tilde{\mathbf{D}}/J$, $q = \tilde{q}/J$, and $\omega = \tilde{\omega}(\mathbf{FN}) \cdot \mathbf{n}/J$, respectively.

The mechanical equilibrium conditions and boundary conditions in the reference configuration (i.e., in the Lagrangian form) have

$$\mathrm{Div}\mathbf{s} + \tilde{\mathbf{b}} = 0, \tag{6a}$$

in the body of the dielectric, and

$$[\mathbf{s}]\mathbf{N} = \tilde{\mathbf{t}}, \tag{6b}$$

on the surface of the dielectric. In Eq. (6a), $\mathbf{s}$ is the nominal stress tensor defined in the reference configuration, and $\tilde{\mathbf{b}}$ is the nominal body force vector defined as the force (such as gravity) applied on a material element divided by the volume of the element in the reference configuration. It should be noted that the effect of electric field has been accounted for in the stress tensor and, therefore, does not appear in the body force.[61–63] In Eq. (6b), $\tilde{\mathbf{t}}$ is the nominal traction vector defined as the force applied on a surface element divided by the area of the element in the reference configuration.

Equivalently, the mechanical equilibrium conditions and boundary conditions in the current configuration (i.e., in the Eulerian form) can be expressed as

$$\mathrm{div}\boldsymbol{\sigma} + \mathbf{b} = 0, \tag{7a}$$

in the body of the dielectric, and

$$[\boldsymbol{\sigma}]\mathbf{n} = \mathbf{t}, \tag{7b}$$

on the surface of the dielectric. In Eq. (7a), $\boldsymbol{\sigma}$ is the true stress tensor defined in the current configuration, and $\mathbf{b}$ is the true body force vector defined as the force applied on a material element divided by the volume of the element in the current configuration (Fig. 3(a)). In Eq. (7b), $\mathbf{t}$ is the true traction vector defined as the force applied on a surface element divided by the area of the element in the current configuration (Fig. 3(a)). In addition, the physical quantities defined in the reference and current configurations in Eqs. (6) and (7) are related via $\boldsymbol{\sigma} = \mathbf{s}\mathbf{F}^T/J$, $\mathbf{b} = \tilde{\mathbf{b}}/J$, and $\mathbf{t} = \tilde{\mathbf{t}}[(\mathbf{FN}) \cdot \mathbf{n}]/J$.

The physical quantities and governing equations for kinematics and equilibrium conditions of deformable dielectrics have been summarized in Tables I and II, respectively.

TABLE I. Summary of physical quantities in the reference and current configurations.

Physical quantity	Reference configuration (nominal quantity)	Current configuration (true quantity)	Relation
Volume of a material element	$\mathrm{d}V$	$\mathrm{d}v$	$\mathrm{d}v = J\,\mathrm{d}V$
Area vector of a surface element	$\mathrm{d}\mathbf{A} = \mathbf{N}\mathrm{d}A$	$\mathrm{d}\mathbf{a} = \mathbf{n}\mathrm{d}a$	$\mathrm{d}\mathbf{a} = J\mathbf{F}^{-T}\mathrm{d}\mathbf{A}$
Electric field vector	$\tilde{\mathbf{E}}$	$\mathbf{E}$	$\mathbf{E} = \mathbf{F}^{-T}\tilde{\mathbf{E}}$
Electric displacement vector	$\tilde{\mathbf{D}}$	$\mathbf{D}$	$\mathbf{D} = \mathbf{F}\tilde{\mathbf{D}}/J$
Body charge density	$\tilde{q}$	q	$q = \tilde{q}/J$
Surface charge density	$\tilde{\omega}$	ω	$\omega = \tilde{\omega}(\mathbf{FN}) \cdot \mathbf{n}/J$
Stress tensor	$\mathbf{s}$	$\boldsymbol{\sigma}$	$\boldsymbol{\sigma} = \mathbf{s}\mathbf{F}^T/J$
Body force vector	$\tilde{\mathbf{b}}$	$\mathbf{b}$	$\mathbf{b} = \tilde{\mathbf{b}}/J$
Surface traction vector	$\tilde{\mathbf{t}}$	$\mathbf{t}$	$\mathbf{t} = \tilde{\mathbf{t}}[(\mathbf{FN}) \cdot \mathbf{n}]/J$
Helmholtz free energy density	$\tilde{W}$	W	$W = \tilde{W}/J$

B. Constitutive law

According to the definition of nominal stress and deformation gradient, associated with a small change of the deformation gradient $\delta\mathbf{F}$, the nominal stress does work $\mathbf{s}\delta\mathbf{F}$; therefore, the nominal stress $\mathbf{s}$ is work conjugate to the deformation gradient $\mathbf{F}$.[60–62,67] Similarly, according to the definition of nominal electric field and nominal electric displacement, associated with a small change of the nominal electric displacement $\delta\tilde{\mathbf{D}}$, the nominal electric field does work $\tilde{\mathbf{E}}\delta\tilde{\mathbf{D}}$; therefore, the nominal electric field $\tilde{\mathbf{E}}$ is work conjugate to the nominal electric displacement $\tilde{\mathbf{D}}$.[60–62,67] It should be noted that the commonly used true electric field $\mathbf{E}$ and true electric displacement $\mathbf{D}$ are actually not work conjugate to each other, when the deformation of dielectrics is large.[63]

Adopting the common practice in electromechanics, we will discuss the constitutive laws of soft dielectrics in the reference configuration based on the work-conjugate pairs. Let us define the nominal Helmholtz free energy density $\tilde{W}$ as the Helmholtz free energy of a material element divided by the volume of the element in the reference configuration. Correspondingly, we have the true Helmholtz free energy density $W = \tilde{W}/J$. It is further assumed that the nominal Helmholtz free energy density is a function of the deformation gradient and the nominal electric displacement, i.e., $\tilde{W}(\mathbf{F}, \tilde{\mathbf{D}})$.

TABLE II. Summary of governing equations in the reference and current configurations.

Governing equations	Reference configuration (Lagrangian form)	Current configuration (Eulerian form)
Gauss's law	$\mathrm{Div}\tilde{\mathbf{D}} = \tilde{q}$	$\mathrm{div}\mathbf{D} = q$
Electrical boundary condition	$\mathbf{N} \cdot [\tilde{\mathbf{D}}] = \tilde{\omega}$	$\mathbf{n} \cdot [\mathbf{D}] = \omega$
Mechanical equilibrium condition	$\mathrm{Div}\mathbf{s} + \tilde{\mathbf{b}} = 0$	$\mathrm{div}\boldsymbol{\sigma} + \mathbf{b} = 0$
Mechanical boundary conditions	$[\mathbf{s}]\mathbf{N} = \tilde{\mathbf{t}}$	$[\boldsymbol{\sigma}]\mathbf{n} = \mathbf{t}$

Therefore, the nominal Helmholtz free energy density, the nominal stress, the deformation gradient, the nominal electric field, and the nominal electric displacement are related via[61–63]

$$\delta\tilde{W}\left(\mathbf{F},\tilde{\mathbf{D}}\right)=\mathbf{s}\delta\mathbf{F}+\tilde{\mathbf{E}}\delta\tilde{\mathbf{D}} \tag{8a}$$

or

$$\mathbf{s}=\frac{\partial\tilde{W}\left(\mathbf{F},\tilde{\mathbf{D}}\right)}{\partial\mathbf{F}}, \tag{8b}$$

$$\tilde{\mathbf{E}}=\frac{\partial\tilde{W}\left(\mathbf{F},\tilde{\mathbf{D}}\right)}{\partial\tilde{\mathbf{D}}}. \tag{8c}$$

From Eq. (8), it can be seen that the form of $\tilde{W}\left(\mathbf{F},\tilde{\mathbf{D}}\right)$ of a deformable dielectric determines its constitutive law.

1. Ideal dielectric model

Since soft dielectrics are mostly constituted of flexible polymer chains with polarizable groups, it is commonly assumed that the electrical polarization of soft dielectrics is liquid-like, independent of their deformation.[68] Further neglecting polarization saturation, we can express the true Helmholtz free energy density of soft dielectrics due to polarization as $W_E=\frac{1}{2\varepsilon}|\mathbf{D}|^2$, where ε is the dielectric constant of the dielectric. A combination of the assumptions of liquid-like polarization and no polarization saturation leads to the ideal dielectric model,[68]

$$\tilde{W}=\tilde{W}_M(\mathbf{F})+\frac{J}{2\varepsilon}|\mathbf{D}|^2, \tag{9a}$$

or, by converting $\mathbf{D}$ into $\tilde{\mathbf{D}}$,

$$\tilde{W}=\tilde{W}_M(\mathbf{F})+\frac{1}{2\varepsilon J}|\mathbf{F}\tilde{\mathbf{D}}|^2, \tag{9b}$$

where the term $\tilde{W}_M(\mathbf{F})$ represents the nominal Helmholtz free energy density due to mechanical deformation of the dielectric. By substituting Eq. (9) into Eq. (8), we reach

$$\mathbf{s}=\frac{\partial\tilde{W}_M}{\partial\mathbf{F}}+\frac{1}{J\varepsilon}(\mathbf{F}\tilde{\mathbf{D}})\otimes\tilde{\mathbf{D}}-\frac{1}{2J\varepsilon}|\mathbf{F}\tilde{\mathbf{D}}|^2\mathbf{F}^{-T}, \tag{10a}$$

$$\tilde{\mathbf{E}}=\frac{1}{\varepsilon J}\mathbf{F}^T(\mathbf{F}\tilde{\mathbf{D}}). \tag{10b}$$

Converting the nominal quantities in Eq. (10) into true quantities, we have

$$\boldsymbol{\sigma}=\frac{\partial\tilde{W}_M}{J\partial\mathbf{F}}\mathbf{F}^T+\frac{1}{\varepsilon}\mathbf{D}\otimes\mathbf{D}-\frac{1}{2\varepsilon}|\mathbf{D}|^2\mathbf{I}, \tag{11a}$$

$$\mathbf{E}=\frac{1}{\varepsilon}\mathbf{D}, \tag{11b}$$

where $\mathbf{I}$ represents the identity tensor. Further substituting Eq. (11b) into Eq. (11a), we obtain

$$\boldsymbol{\sigma}=\frac{\partial\tilde{W}_M}{J\partial\mathbf{F}}\mathbf{F}^T+\frac{1}{\varepsilon}\mathbf{E}\otimes\mathbf{E}-\frac{1}{2\varepsilon}|\mathbf{E}|^2\mathbf{I}, \tag{12}$$

where $\frac{1}{\varepsilon}\mathbf{E}\otimes\mathbf{E}-\frac{1}{2\varepsilon}|\mathbf{E}|^2\mathbf{I}$ is the well-known Maxwell stress tensor in dielectrics.[58–60] It can be seen that the Maxwell stress tensor is a consequence of the ideal dielectric model.[68]

2. Incompressible neo-Hookean model

Since the bulk moduli of elastomers and gels are generally much higher than their shear moduli, soft dielectrics are commonly regarded to be incompressible. A widely used constitutive law for the mechanical properties of soft dielectrics is the incompressible neo-Hookean model,

$$\tilde{W}_M=\frac{1}{2}\mu[\mathrm{trace}(\mathbf{F}^T\mathbf{F})-3]-p(J-1), \tag{13}$$

where μ is the initial shear modulus of the dielectric and p is a Lagrangian multiplier that imposes the incompressibility condition. Substituting Eq. (13) into Eqs. (10a) and (11a) gives

$$\mathbf{s}=\mu\mathbf{F}-pJ\mathbf{F}^{-T}+\frac{1}{J\varepsilon}(\mathbf{F}\tilde{\mathbf{D}})\otimes\tilde{\mathbf{D}}-\frac{1}{2J\varepsilon}|\mathbf{F}\tilde{\mathbf{D}}|^2\mathbf{F}^{-T} \tag{14}$$

and

$$\boldsymbol{\sigma}=\frac{\mu\mathbf{F}\mathbf{F}^T}{J}-p\mathbf{I}+\frac{1}{\varepsilon}\mathbf{D}\otimes\mathbf{D}-\frac{1}{2\varepsilon}|\mathbf{D}|^2\mathbf{I}. \tag{15}$$

From Eq. (15), it can be seen that the Lagrangian multiplier p represents the hydrostatic pressure in the dielectric, which is to be determined by boundary conditions.

C. Stability against linear perturbation

The constitutive law, Eq. (8), can be further expressed in the incremental form as[68–70]

$$\begin{bmatrix}\delta\mathbf{s}\\ \delta\tilde{\mathbf{E}}\end{bmatrix}=\mathbf{H}\begin{bmatrix}\delta\mathbf{F}\\ \delta\tilde{\mathbf{D}}\end{bmatrix}, \tag{16a}$$

where $\mathbf{H}$ is the Hessian matrix,

$$\mathbf{H}=\begin{bmatrix}\dfrac{\partial^2\tilde{W}\left(\mathbf{F},\tilde{\mathbf{D}}\right)}{\partial\mathbf{F}\partial\mathbf{F}} & \dfrac{\partial^2\tilde{W}\left(\mathbf{F},\tilde{\mathbf{D}}\right)}{\partial\tilde{\mathbf{D}}\partial\mathbf{F}}\\ \dfrac{\partial^2\tilde{W}\left(\mathbf{F},\tilde{\mathbf{D}}\right)}{\partial\mathbf{F}\partial\tilde{\mathbf{D}}} & \dfrac{\partial^2\tilde{W}\left(\mathbf{F},\tilde{\mathbf{D}}\right)}{\partial\tilde{\mathbf{D}}\partial\tilde{\mathbf{D}}}\end{bmatrix}, \tag{16b}$$

and $\delta\mathbf{s}$,$\delta\tilde{\mathbf{E}}$, $\delta\mathbf{F}$, and $\delta\tilde{\mathbf{D}}$ represent small increments of nominal stress, nominal electric field, deformation gradient, and nominal electric displacement, respectively. The nominal stress and nominal electric field can be regarded as the generalized loads, and the deformation gradient and nominal electric displacement as the response of the dielectric to the loads. Thermodynamics dictates that the stability of the dielectric against small increments of the loads (i.e., linear perturbation) requires the Hessian matrix $\mathbf{H}$ to be positive definite. Therefore, a soft dielectric becomes unstable against linear perturbation when

$$\det\mathbf{H}=0. \tag{17}$$

It should be noted that, in some cases, one equilibrium state of a soft dielectric may be stable against linear

perturbation, but it can become unstable under finite fluctuation.[71,72] We will discuss various modes of instabilities in Sec. IV of the paper.

III. SOFT-DIELECTRIC FILMS

Soft dielectrics are mostly used in the form of thin films. The two surfaces of soft-dielectric films are usually coated with electrodes on which electrical voltages are applied. In rare cases, the voltage can also be induced by depositing charges of different signs on surfaces of a dielectric film.[73–75] Since the lateral dimensions of a film are much larger than its thickness, the electric field can be regarded as homogeneous through the thickness of the film in regions far away from electrode edges. Therefore, the nominal electric field in a dielectric film can be expressed as[76]

$$\tilde{E}_1 = \tilde{E}_2 = 0, \quad \tilde{E}_3 = \frac{\Phi}{H}, \tag{18}$$

where $\tilde{E}_i$ is the nominal electric field in the ith direction, Φ is the applied voltage, and H is the thickness of the film in the reference configuration (Fig. 3(b)). In addition, soft dielectric films frequently undergo homogeneous deformation without rotation, which gives the deformation gradient

$$\mathbf{F} = \begin{bmatrix} \lambda_1 & 1 & 1 \\ 1 & \lambda_2 & 1 \\ 1 & 1 & \lambda_3 \end{bmatrix}, \tag{19}$$

where λ_i is the principle stretch in the ith direction, and $J = \lambda_1\lambda_2\lambda_3$ (Fig. 3(b)).

Further taking the soft dielectric to be an ideal dielectric, we can express the nominal Helmholtz free energy density as based on Eq. (9),

$$\tilde{W} = \tilde{W}_M(\lambda_1, \lambda_2, \lambda_3) + \frac{\lambda_3}{2\lambda_1\lambda_2\varepsilon}\tilde{D}_3^2, \tag{20}$$

and the constitutive law as

$$s_1 = \frac{\partial \tilde{W}}{\partial \lambda_1} = \frac{\partial \tilde{W}_M}{\partial \lambda_1} - \frac{\lambda_3}{2\lambda_1^2\lambda_2\varepsilon}\tilde{D}_3^2, \tag{21a}$$

$$s_2 = \frac{\partial \tilde{W}}{\partial \lambda_2} = \frac{\partial \tilde{W}_M}{\partial \lambda_2} - \frac{\lambda_3}{2\lambda_1\lambda_2^2\varepsilon}\tilde{D}_3^2, \tag{21b}$$

$$s_3 = \frac{\partial \tilde{W}}{\partial \lambda_3} = \frac{\partial \tilde{W}_M}{\partial \lambda_3} + \frac{1}{2\lambda_1\lambda_2\varepsilon}\tilde{D}_3^2, \tag{21c}$$

$$\tilde{E}_3 = \frac{\partial \tilde{W}}{\partial \tilde{D}_3} = \frac{\lambda_3}{\varepsilon\lambda_1\lambda_2}\tilde{D}_3, \tag{21d}$$

where s_i is the normal nominal stress in the ith direction, and $\tilde{D}_i$ is the nominal electric displacement in the ith direction. Here, the shear components of the nominal stress are 0, and $\tilde{D}_1 = \tilde{D}_2 = 0$. According to the electrical boundary condition Eq. (4b), we have $\tilde{D}_3 = Q/A$, where Q is the charge on either electrode and A the area of the electrode in the reference configuration. Therefore, from Eqs. (18) and (21d), the capacitance of an ideal soft dielectric capacitor can be calculated as $C = \varepsilon\lambda_1\lambda_2 A/(\lambda_3 H)$. It can be seen that the capacitance is significantly dependent on the deformation of the soft dielectric. Such property has been used to design sensors based on dielectric elastomers capable of large deformation.[34–36]

Further converting the nominal quantities in Eq. (21) into true quantities, we have

$$\sigma_1 = \frac{\partial \tilde{W}_M}{\lambda_2\lambda_3\partial\lambda_1} - \frac{1}{2\varepsilon}D_3^2, \tag{22a}$$

$$\sigma_2 = \frac{\partial \tilde{W}_M}{\lambda_1\lambda_3\partial\lambda_2} - \frac{1}{2\varepsilon}D_3^2, \tag{22b}$$

$$\sigma_3 = \frac{\partial \tilde{W}_M}{\lambda_1\lambda_2\partial\lambda_3} + \frac{1}{2\varepsilon}D_3^2, \tag{22c}$$

$$E_3 = \frac{1}{\varepsilon}D_3, \tag{22d}$$

where σ_i is the normal true stress in the ith direction, and E_i and D_i are the true electric field and true electric displacement in the ith direction. It is evident that the shear components of the true stress are 0, and $E_1 = E_2 = D_1 = D_2 = 0$.

If the ideal soft dielectric film further follows the incompressible neo-Hookean model, i.e., $\tilde{W}_M = \mu(\lambda_1^2 + \lambda_2^2 + \lambda_3^2 - 3)/2 - p(\lambda_1\lambda_2\lambda_3 - 1)$, we can express the constitutive law as

$$s_1 = \mu\lambda_1 - p\lambda_2\lambda_3 - \frac{\lambda_3}{2\lambda_1^2\lambda_2\varepsilon}\tilde{D}_3^2, \tag{23a}$$

$$s_2 = \mu\lambda_2 - p\lambda_1\lambda_3 - \frac{\lambda_3}{2\lambda_1\lambda_2^2\varepsilon}\tilde{D}_3^2, \tag{23b}$$

$$s_3 = \mu\lambda_3 - p\lambda_1\lambda_2 + \frac{1}{2\lambda_1\lambda_2\varepsilon}\tilde{D}_3^2, \tag{23c}$$

$$\tilde{E}_3 = \frac{\lambda_3}{\varepsilon\lambda_1\lambda_2}\tilde{D}_3, \tag{23d}$$

and

$$\sigma_1 = \mu\lambda_1^2 - p - \frac{1}{2\varepsilon}D_3^2, \tag{24a}$$

$$\sigma_2 = \mu\lambda_2^2 - p - \frac{1}{2\varepsilon}D_3^2, \tag{24b}$$

$$\sigma_3 = \mu\lambda_3^2 - p + \frac{1}{2\varepsilon}D_3^2, \tag{24c}$$

$$E_3 = \frac{1}{\varepsilon}D_3. \tag{24d}$$

By substituting Eq. (24d) into Eqs. (24a)–(24c), we further obtain

$$\sigma_1 = \mu\lambda_1^2 - p - \frac{\varepsilon}{2}E_3^2, \tag{25a}$$

$$\sigma_2 = \mu\lambda_2^2 - p - \frac{\varepsilon}{2}E_3^2, \tag{25b}$$

$$\sigma_3 = \mu\lambda_3^2 - p + \frac{\varepsilon}{2}E_3^2. \tag{25c}$$

TABLE III. Summary of the ideal-dielectric laws in the reference and current configurations.

	Reference configuration (Lagrangian form)	Current configuration (Eulerian form)	Relation
General ideal dielectric	$\mathbf{s}=\frac{\partial \tilde{W}_M}{\partial \mathbf{F}}+\frac{1}{J\varepsilon}(\mathbf{F}\tilde{\mathbf{D}})\otimes\tilde{\mathbf{D}}-\frac{1}{2J\varepsilon}\lvert\mathbf{F}\tilde{\mathbf{D}}\rvert^2\mathbf{F}^{-T}$, $\tilde{\mathbf{E}}=\frac{1}{\varepsilon J}\mathbf{F}^T(\mathbf{F}\tilde{\mathbf{D}})$	$\boldsymbol{\sigma}=\frac{\partial \tilde{W}_M}{J\partial \mathbf{F}}\mathbf{F}^T+\frac{1}{\varepsilon}\mathbf{D}\otimes\mathbf{D}-\frac{1}{2\varepsilon}\lvert\mathbf{D}\rvert^2\mathbf{I}$, $\mathbf{E}=\frac{1}{\varepsilon}\mathbf{D}$	$\boldsymbol{\sigma}=\mathbf{s}\mathbf{F}^T/J$, $\mathbf{E}=\mathbf{F}^{-T}\tilde{\mathbf{E}}$, $\mathbf{D}=\mathbf{F}\tilde{\mathbf{D}}/J$
Ideal dielectric film	$s_1=\frac{\partial \tilde{W}_M}{\partial \lambda_1}-\frac{\lambda_3}{2\lambda_1^2\lambda_2\varepsilon}\tilde{D}_3^2$, $s_2=\frac{\partial \tilde{W}_M}{\partial \lambda_2}-\frac{\lambda_3}{2\lambda_1\lambda_2^2\varepsilon}\tilde{D}_3^2$, $s_3=\frac{\partial \tilde{W}_M}{\partial \lambda_3}+\frac{1}{2\lambda_1\lambda_2\varepsilon}\tilde{D}_3^2$, $\tilde{E}_3=\frac{\lambda_3}{\varepsilon\lambda_1\lambda_2}\tilde{D}_3$	$\sigma_1=\frac{\partial \tilde{W}_M}{\lambda_2\lambda_3\partial \lambda_1}-\frac{1}{2\varepsilon}D_3^2$, $\sigma_2=\frac{\partial \tilde{W}_M}{\lambda_1\lambda_3\partial \lambda_2}-\frac{1}{2\varepsilon}D_3^2$, $\sigma_3=\frac{\partial \tilde{W}_M}{\lambda_1\lambda_2\partial \lambda_3}+\frac{1}{2\varepsilon}D_3^2$, $E_3=\frac{1}{\varepsilon}D_3$	$\sigma_1=s_1/(\lambda_2\lambda_3)$, $\sigma_2=s_2/(\lambda_1\lambda_3)$, $\sigma_3=s_3/(\lambda_1\lambda_2)$, $E_3=\tilde{E}_3/\lambda_3$, $D_3=\tilde{D}_3/(\lambda_1\lambda_2)$
Incompressible neo-Hookean ideal dielectric film ($\lambda_1\lambda_2\lambda_3=1$)	$s_1=\mu\lambda_1-p\lambda_2\lambda_3-\frac{\lambda_3}{2\lambda_1^2\lambda_2\varepsilon}\tilde{D}_3^2$, $s_2=\mu\lambda_2-p\lambda_1\lambda_3-\frac{\lambda_3}{2\lambda_1\lambda_2^2\varepsilon}\tilde{D}_3^2$, $s_3=\mu\lambda_3-p\lambda_1\lambda_2+\frac{1}{2\lambda_1\lambda_2\varepsilon}\tilde{D}_3^2$, $\tilde{E}_3=\frac{\lambda_3}{\varepsilon\lambda_1\lambda_2}\tilde{D}_3$	$\sigma_1=\mu\lambda_1^2-p-\frac{1}{2\varepsilon}D_3^2$, $\sigma_2=\mu\lambda_2^2-p-\frac{1}{2\varepsilon}D_3^2$, $\sigma_3=\mu\lambda_3^2-p+\frac{1}{2\varepsilon}D_3^2$, $E_3=\frac{1}{\varepsilon}D_3$	$\sigma_1=s_1\lambda_1$, $\sigma_2=s_2\lambda_2$, $\sigma_3=s_3\lambda_3$, $E_3=\tilde{E}_3/\lambda_3$, $D_3=\tilde{D}_3\lambda_3$

Note that $\lambda_1\lambda_2\lambda_3=1$ in Eqs. (23)–(25), due to the incompressibility condition. The constitutive relations of soft dielectrics that follow the ideal dielectric law have been summarized in Table III.

In addition, from Eq. (16), the Hessian matrix for soft-dielectric films can be expressed as

$$\mathbf{H}=\begin{bmatrix} \frac{\partial^2\tilde{W}}{\partial\lambda_1^2} & \frac{\partial^2\tilde{W}}{\partial\lambda_1\lambda_2} & \frac{\partial^2\tilde{W}}{\partial\lambda_1\lambda_3} & \frac{\partial^2\tilde{W}}{\partial\lambda_1\tilde{D}_3} \\ \frac{\partial^2\tilde{W}}{\partial\lambda_2\lambda_1} & \frac{\partial^2\tilde{W}}{\partial\lambda_2^2} & \frac{\partial^2\tilde{W}}{\partial\lambda_2\lambda_3} & \frac{\partial^2\tilde{W}}{\partial\lambda_2\tilde{D}_3} \\ \frac{\partial^2\tilde{W}}{\partial\lambda_3\lambda_1} & \frac{\partial^2\tilde{W}}{\partial\lambda_3\lambda_2} & \frac{\partial^2\tilde{W}}{\partial\lambda_3^2} & \frac{\partial^2\tilde{W}}{\partial\lambda_3\tilde{D}_3} \\ \frac{\partial^2\tilde{W}}{\partial\tilde{D}_3\lambda_1} & \frac{\partial^2\tilde{W}}{\partial\tilde{D}_3\lambda_2} & \frac{\partial^2\tilde{W}}{\partial\tilde{D}_3\lambda_3} & \frac{\partial^2\tilde{W}}{\partial\tilde{D}_3^2} \end{bmatrix}. \quad (26)$$

As discussed in Sec. II C, when $\det\mathbf{H}$ of Eq. (26) reaches zero, the soft-dielectric film will become unstable against linear perturbation. In addition, the governing equations for the equilibrium and stability of soft-dielectric films may be simplified, dependent on the symmetry in deformation of soft-dielectric films.

IV. THREE GENERIC MODES OF DEFORMATION AND INSTABILITIES

The electrodes on soft dielectric films can be either compliant or rigid. Conductive greases[6,17] and powders,[77,78] thin conductive films,[79] wrinkled or crumpled conductive films,[20,77] meshes of carbon nanotubes[80–83] and metallic nanowires,[84–86] liquid metal,[14,87] conductive solutions,[49,71,77] and conductive gels[88,89] are examples of compliant electrodes, which do not constrain deformation of soft dielectrics. Rigid electrodes typically include conductive (e.g., metals or conductive epoxy) thick slabs or wires, which constrain deformation of the soft dielectrics' surfaces bonded on them. Therefore, according to the type of electrode coated on each surface of a soft dielectric film, three generic types of mechanical boundary conditions can be classified: no mechanical constraint on either surface (Fig. 4(a)), mechanical constraint on only one surface (Fig. 4(b)), and mechanical constraint on both surfaces (Fig. 4(c)). Consequently, we will discuss three generic modes of deformation and instabilities of soft dielectrics based on the mechanical constraints (Fig. 4).

A. Mode I: Thinning and pull-in instability

The deformation of soft dielectric films coated with compliant electrodes on both surfaces is unconstrained by the electrodes. This configuration has been adopted in most dielectric-elastomer transducers[19] (e.g., actuators, sensors, and energy harvesters) and some polymer capacitors.[11,12,90] When a voltage is applied on an unconstrained soft-dielectric film, its thickness becomes thinner and area becomes larger, undergoing a thinning process (e.g., Fig. 5(a)). As the film thins down, the same applied voltage can induce a higher true electric field, resulting in a higher Maxwell stress that further deforms the film [see Eq. (25)].

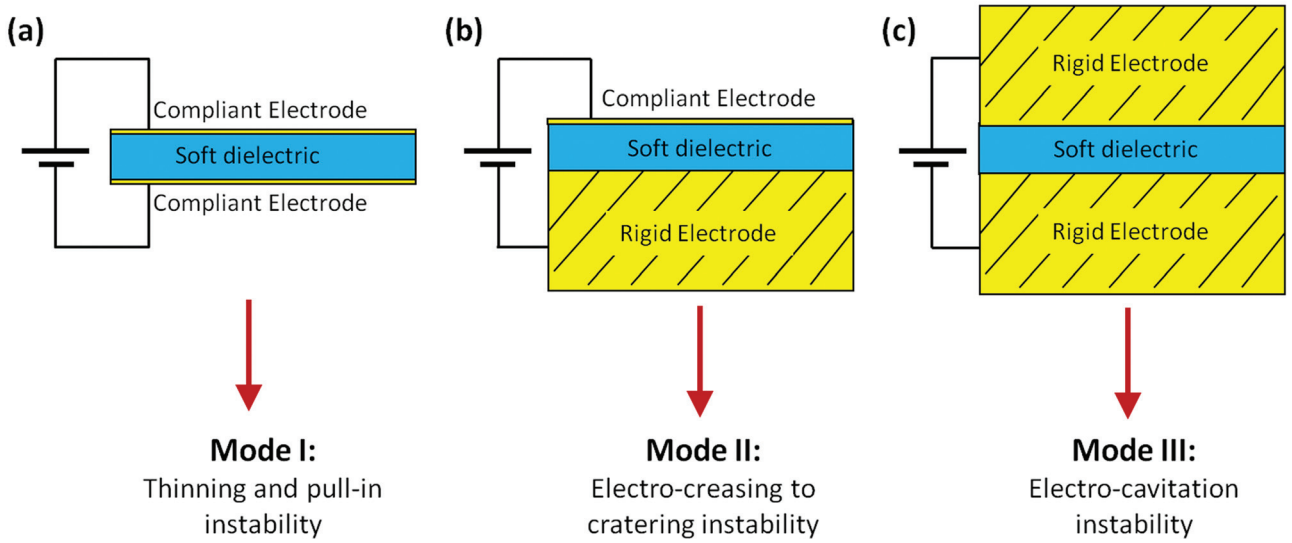

FIG. 4. Three types of mechanical constraints on soft-dielectric films: (a) no mechanical constraint with compliant electrodes on both surfaces, (b) one-side mechanical constraint with rigid electrode bonded on one surface and complaint electrode on the other, and (c) two-side mechanical constraint with rigid electrodes bonded on both surfaces. Based on the three types of mechanical constraints, the deformation and instabilities of soft dielectrics can be classified into three generic modes.

At a critical point, the positive feedback may cause the elastomer to thin down abruptly, resulting in the pull-in instability.[11,69] For example, Fig. 5(b) illustrates that a dielectric-elastomer film, when subjected to the pull-in instability, thins down drastically and becomes wrinkled, due to constraints from surrounding regions.[91] Shortly after the pull-in instability, the dielectric elastomer film breaks down.[91]

1. Experimental method

The thinning and pull-in instability of soft dielectrics was first proposed by Stark and Garton.[11] Assuming soft dielectric to be a linear elastic material, they derived that the critical electric field for pull-in instability scales with square root of the modulus of the dielectric. To validate the model, they measured the breakdown nominal electric fields of irradiated polythene films with different moduli by varying temperature and observed that the breakdown nominal electric field indeed increases monotonically with the modulus of polythene.

Following the pioneer work by Stark and Garton,[11] a number of experiments have been carried out to investigate the relations between breakdown fields of polymers and their mechanical properties.[12,92–103] Despite the significant amount of data, these experiments only validated the pull-in instability indirectly, because electrical breakdown instead of the instability of polymers was observed. Recent development of dielectric-elastomer transducers escalates the interests in understanding pull-in instability as a major failure mode of the transducers, further calling for direct observation of pull-in instability. Using a viscoelastic elastomer—VHB, Plante and Dubowsky[91] and Keplinger *et al.*[104] directly observed drastic thinning of the elastomer film under critical electric fields, right before electrical breakdown (e.g., Fig. 5(b)). Wrinkling of the soft-dielectric films were also commonly observed during thinning and/or pull-in instability.[91,104,105]

2. Theoretical analysis

Theoretical models for unconstrained soft-dielectric films are based on the electromechanics of deformable dielectrics discussed in Secs. II and III. Since soft dielectrics are commonly incompressible and the deformation in two in-

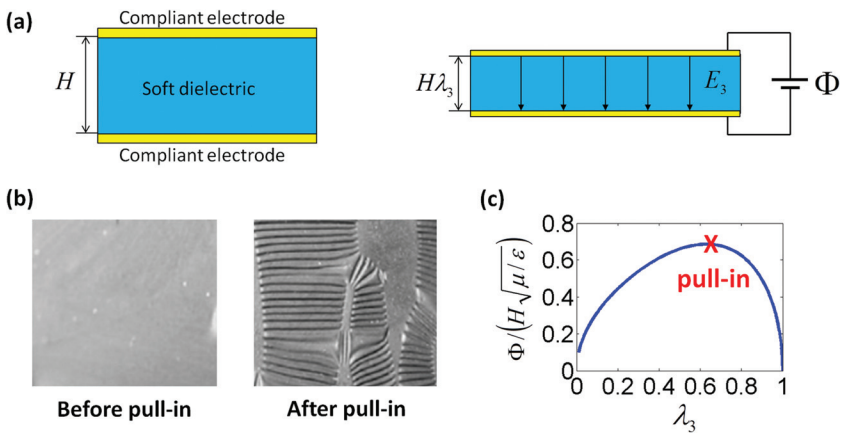

FIG. 5. Mode I, thinning and pull-in instability in unconstrained soft dielectric films: (a) schematics of the thinning under voltage, (b) experimental observation of the pull-in instability with drastic thinning of the soft-dielectric film [Reprinted with permission from J. S. Plante and S. Dubowsky, Int. J. Solids Struct. **43**, 7727–7751 (2006). Copyright 2006 Elsevier[91]], and (c) theoretical model for the deformation of the film, λ_3, as a function of the applied voltage, Φ. The critical point for the pull-in instability is indicated as a cross.

plane directions without applied forces are symmetric, we have $\lambda_1 = \lambda_2 = \lambda_3^{-1/2}$. Further assuming the soft dielectric follows the neo-Hookean ideal dielectric model, we have the nominal Helmholtz free energy of the dielectric as[69]

$$\tilde{W} = \frac{1}{2}\mu\left(\lambda_3^2 + 2\lambda_3^{-1} - 3\right) + \frac{\lambda_3^2\tilde{D}_3^2}{2\varepsilon}. \tag{27}$$

From Eq. (8), we can calculate the nominal stress and nominal electric field,

$$s_3 = \mu\left(\lambda_3 - \lambda_3^{-2}\right) + \frac{\lambda_3\tilde{D}_3^2}{\varepsilon}, \tag{28a}$$

$$\tilde{E}_3 = \frac{\lambda_3^2\tilde{D}_3}{\varepsilon}. \tag{28b}$$

Further considering no force is applied on the surface of the dielectric film, i.e., $s_3 = 0$, we can obtain the relation between the applied voltage and the deformation

$$\frac{\Phi}{H} = \tilde{E}_3 = \sqrt{\frac{\mu}{\varepsilon}\left(\lambda_3 - \lambda_3^4\right)}, \tag{29}$$

which has been plotted on Fig. 5(c). Note that the same relation can be obtained by substituting $\lambda_1 = \lambda_2 = \lambda_3^{-1/2}$ into Eq. (23) and setting $s_1 = s_2 = s_3 = 0$. Furthermore, the Hessian matrix can be calculated as

$$\mathbf{H} = \begin{bmatrix} \mu\left(1 + 2\lambda_3^{-3}\right) + \dfrac{\tilde{D}_3^2}{\varepsilon} & \dfrac{2\lambda_3\tilde{D}_3}{\varepsilon} \\ \dfrac{2\lambda_3\tilde{D}_3}{\varepsilon} & \dfrac{\lambda_3^2}{\varepsilon} \end{bmatrix}. \tag{30}$$

By setting $\det\mathbf{H} = 0$, we obtain that the critical point for the pull-in instability is at $\lambda_{3c} \approx 0.63$ and $\tilde{E}_{3c} \approx 0.69\sqrt{\mu/\varepsilon}$, which gives $E_{3c} \approx 1.1\sqrt{\mu/\varepsilon}$. Note that the critical point is also corresponding to the peak on the curve of $\tilde{E}_3$ vs. λ_3 from Eq. (29) (Fig. 5(c)).

In addition to the neo-Hookean model, the pull-in instability in soft dielectrics has been analyzed with various other constitutive models.[11,106–116] For example, it has been found that the critical point for pull-in instability in linear-elastic ideal dielectric is similar to that of neo-Hookean ideal dielectric.[11] On the other hand, the critical point for pull-in instability in semicrystalline or glassy polymers, characterized by elasto-plastic models, can be distinctly different from that of neo-Hookean ideal dielectrics.[12,13]

Furthermore, from the above analysis, it is evident that a neo-Hookean soft-dielectric film can only expand its area by ~37% under voltage before the pull-in instability (i.e., $\lambda_{3c} \approx 0.63$). The limited deformation seems to be contradictory with the observation that dielectric-elastomer actuators can readily achieve area actuation strain over 100%. In fact, over a few decades, the pull-in instability indeed restrained the actuation strains of soft dielectrics below 40%.[6] Now, it is understood that the actuation strain can be greatly enhanced by preventing or harnessing the pull-in instability, which will be discuss in Secs. V and VI of the paper, respectively.

B. Mode II: Electro-creasing to cratering instabilities

In many cases, only one surface of a soft-dielectric film is mechanically constrained (e.g., Fig. 6(a)). Examples include insulating polymers or polymer capacitors with thick rigid electrode on one surface but thin conductive film or infiltrated water on the other surface. In addition, this configuration of soft dielectrics enables a recently developed technology, dynamic electro-lithography, which is capable of dynamically generating topographical patterns over large-area curved surfaces with voltages.[51]

Since the thick rigid electrode constrains lateral expansion of dielectric film, the dielectric cannot homogeneously thin down as in the unconstrained case (e.g., Fig. 5(a)). Instead, as the applied voltage increases, the dielectric film maintains its initially undeformed configuration. When the voltage reaches a critical value, regions of the dielectric surface will fold against itself to form a pattern of creases (Figs. 6(a) and 6(c)).[71] As the voltage increases, the pattern of creases coarsens by increasing their sizes (i.e., length and width) and decreasing their density (i.e., number of creases per area). As the voltage further rises, the center regions of some creases strikingly open, and a pattern of coexistent creases and craters form in the soft-dielectric film. All creases eventually deform into craters with further increase of the voltage (Figs. 6(a) and 6(c)). The electro-creasing to cratering instability induces inhomogeneous deformation and non-uniform electric fields in the soft dielectric (Fig. 6(a)).

1. Experimental method

Since soft dielectrics usually breakdown electrically right after the onset of the electro-creasing instability, experimental observation of the instability has been challenging. Wang *et al.* recently invented an experimental method that enables direct observation of the electro-creasing to cratering instability.[49,71] The new method combined a transparent liquid electrode (e.g., NaCl solution) above the soft dielectric (e.g., silicone elastomer) and a rigid dielectric substrate (e.g., Teflon) that bonds the soft dielectric with a metal electrode as demonstrated in Fig. 6(b). The transparent liquid electrode can deform conformally with the soft dielectric and also enables the observation of the soft-dielectric surface from an optical microscope lens above it (Fig. 6(b)). On the other hand, the rigid dielectric substrate prevents the electric field in the deformed polymer from becoming excessively high to avoid electrical breakdown. Since the electric field in soft-dielectric film is uniform in regions far away from creases and craters, this uniform electric field is defined as the applied electric field on the soft dielectric, i.e.,

$$\tilde{E}_3 = E_3 = \frac{\Phi}{H + H_s\varepsilon/\varepsilon_s}, \tag{31}$$

where H_s and ε_s are the thickness and permittivity of the rigid substrate, respectively. Once the applied electric field reaches a critical value E_{3c} (or $\tilde{E}_{3c}$), the electro-creasing instability will set in.[49,71] As the applied electric field further increases, the electro-creasing instability can transit to the electro-cratering instability.

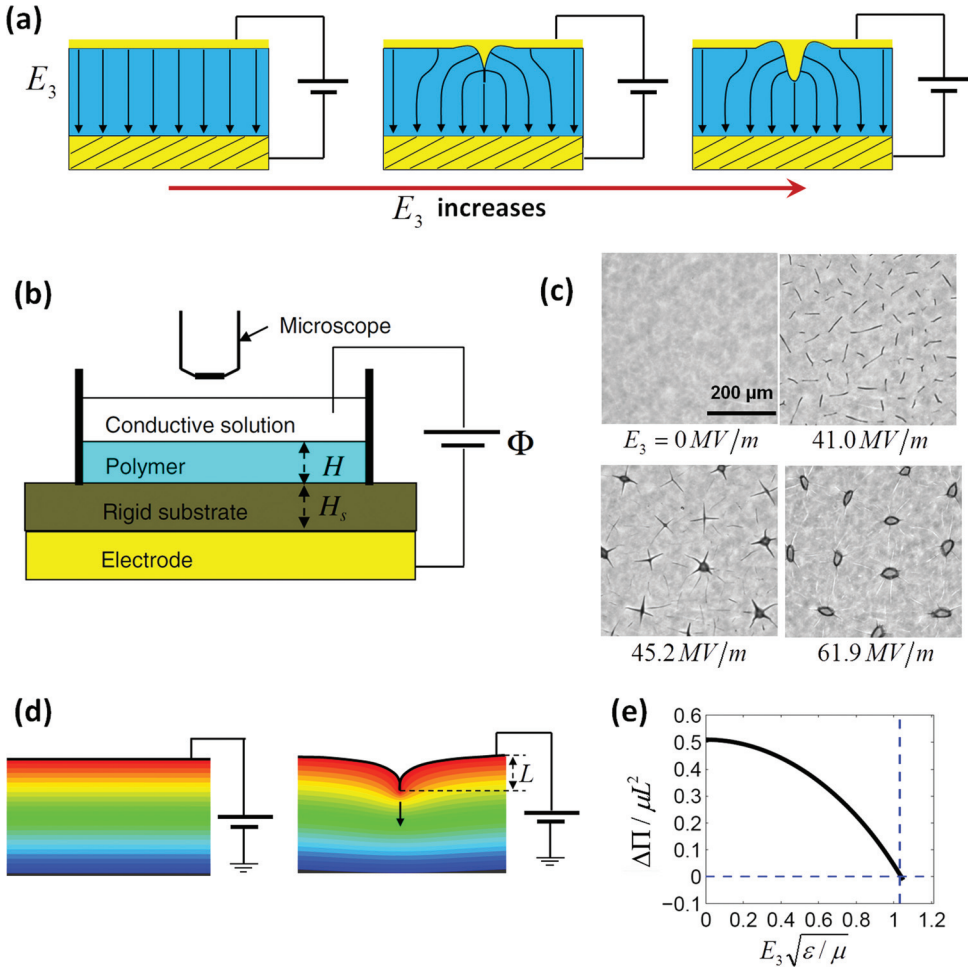

FIG. 6. Mode II, electro-creasing to cratering instability in one-side-constrained soft-dielectric films: (a) schematics of the electro-creasing to cratering instability, (b) experimental setup for observation of the instability, (c) optical microscopic images of the process of deformation and instability, and (d) and (e) theoretical prediction of the onset of the electro-creasing. The counters in (d) represent electrical potential in the soft dielectric at the flat and creased states. The difference of Gibbs free energy of the two states, $\Delta\Pi$, is plotted as a function of the applied electric field, E_3, in (e). Once the difference reaches zero, the electro-creasing instability sets in. Reprinted with permission from Wang *et al.*, Phys. Rev. Lett. **106**, 118301 (2011). Copyright 2011 American Physical Society.[71]

2. Theoretical analysis

Prior to the electro-creasing instability, the incompressible soft-dielectric film is undeformed on the rigid substrate. Since the top surface of the soft-dielectric film is traction free, the true stresses in the film can be calculated from Eq. (25) as

$$\sigma_1 = \sigma_2 = -\varepsilon E_3^2, \tag{32a}$$

$$\sigma_3 = 0. \tag{32b}$$

From Eq. (32), it can be seen that the soft-dielectric film is under in-plane compressive stress induced by the applied electric field. When the electric field reaches a critical value E_{3c} (or $\tilde{E}_{3c}$), creases set in the soft dielectric.

Creasing instability is distinctly different from wrinkling instability.[117,118] Regardless of the size of a crease, material around the crease tip undergoes finite deformation.[117,119] Therefore, the linear-stability methods discussed in Sec. II C and other references[120–123] are not applicable to the analysis of electro-creasing instability, because these methods assume small deformation.[117,119,124,125] Instead, Wang *et al.* adopted the Maxwell stability criterion to predict the onset of the electro-creasing instability by comparing the Gibbs free energy of the soft-dielectric system at the flat and creased states.[49,71,119] The Gibbs free energy in a unit thickness of a region in the soft dielectric (Fig. 6(d)) can be expressed as

$$\Pi = \int_A \frac{1}{2}\mu[\mathrm{trace}(\mathbf{F}^T\mathbf{F}) - 3]dA + \int_A \frac{1}{2}\varepsilon|\mathbf{E}|^2 dA - \int_S \Phi\omega dS, \tag{33}$$

where A and S are the area and contour of the region. The first term of Eq. (33) gives the elastic energy of the neo-Hookean material, and the second and third terms give the electrostatic potential energy of the region.

When the film is in a flat state, the elastic energy is zero and the Gibbs free energy per unit thickness can be calculated as $\Pi_{flat} = -A\varepsilon E_3^2/2$, where E_3 is the applied electric field given by Eq. (31). To calculate the Gibbs free energy at the creased state, a downward displacement L is prescribed on a line on the top surface of the region to form a crease (Fig. 6(d)).[126] At the creased state, the deformation and electric field are non-uniform in the region, and the Gibbs free

energy of the creased state Π_{crease} needs to be calculated with numerical methods, such as finite element method.[49,71,127] The size of the calculation domain is set to be much larger than the size of the crease so that L is the only length scale relevant in comparing the potential energies in the flat and creased states. Therefore, dimensional consideration determines that the Gibbs free energy difference has a form[49,71,119]

$$\Delta\Pi = \Pi_{crease} - \Pi_{flat} = \mu L^2 f\left(E_3\sqrt{\varepsilon/\mu}\right), \qquad (34)$$

where E_3 is the applied (homogeneous) electric field far away from the crease. As the applied field reaches a critical value E_{3c}, the Gibbs free energy difference becomes 0 and the electro-creasing instability sets in. As shown in Fig. 6(e), the theoretical calculation gives $E_{3c} \approx 1.03\sqrt{\mu/\varepsilon}$, which is slightly lower than the critical true electric field for pull-in instability. As the applied electric field further increases, the transition from electro-creasing to electro-cratering can be simulated by numerical models.[127,128]

C. Mode III: Electro-cavitation instability

In many capacitors and insulating cables, both surfaces of soft dielectric films are constrained by thick and rigid electrodes. Ideally, the mechanical constraints should prevent any deformation of the soft dielectric films. However, defects such as air bubbles, water drops, and impurities can be trapped in soft dielectrics during manufacturing and processing of the dielectrics. These defects can deform and become unstable under applied voltages, leading to inhomogeneous deformation in dielectrics around the defects.[72,129]

Finis and Claudi[129] and Wang *et al.*[72] observed that defects such as air bubbles and water drops can significantly reduce the measured breakdown electric fields of soft dielectrics including silicone rubbers and gels. In addition, Wang *et al.* observed and analyzed the deformation and instability of water drops trapped in soft dielectric films with both surfaces mechanically constrained (Fig. 7(a)).[72] As the applied electric field increases, a spherical drop in the constrained soft-dielectric film gradually deforms into a spheroid. When the electric field reaches a critical value, the drop suddenly becomes unstable and forms sharp tips on its apexes, giving the electro-cavitation instability.[72] As the electric field is further ramped up, the sharp tips open up and eventually deform into the shape of a long tube in the dielectric (Fig. 7(c)).

1. Experimental method

Since the electro-cavitation instability subsequently leads to electrical breakdown of soft dielectrics, observation of the instability requires prevention or significant delay of electrical breakdown. Wang *et al.* invented a method to use transparent rigid dielectric substrates to prevent electrical breakdown of soft dielectrics, which makes direct observation of the electro-cavitation instability possible.[72] They fabricated a layer of a soft dielectric (e.g., silicone rubber) that traps single or multiple drops of a conductive solution (e.g., NaCl). The radius of the drop was set to be much smaller than the thickness of the soft dielectric. They then sandwiched the soft dielectric between two rigid transparent dielectric films (e.g., Teflon) coated with transparent electrodes (e.g., gold thin films) (Fig. 7(b)). The rigid films suppress overall deformation (i.e., thinning) and electric breakdown of the soft dielectric. As a voltage is applied between the electrodes, the electric field far away from the drop is uniform and is regarded as the applied electric field E_3 (or $\tilde{E}_3$),

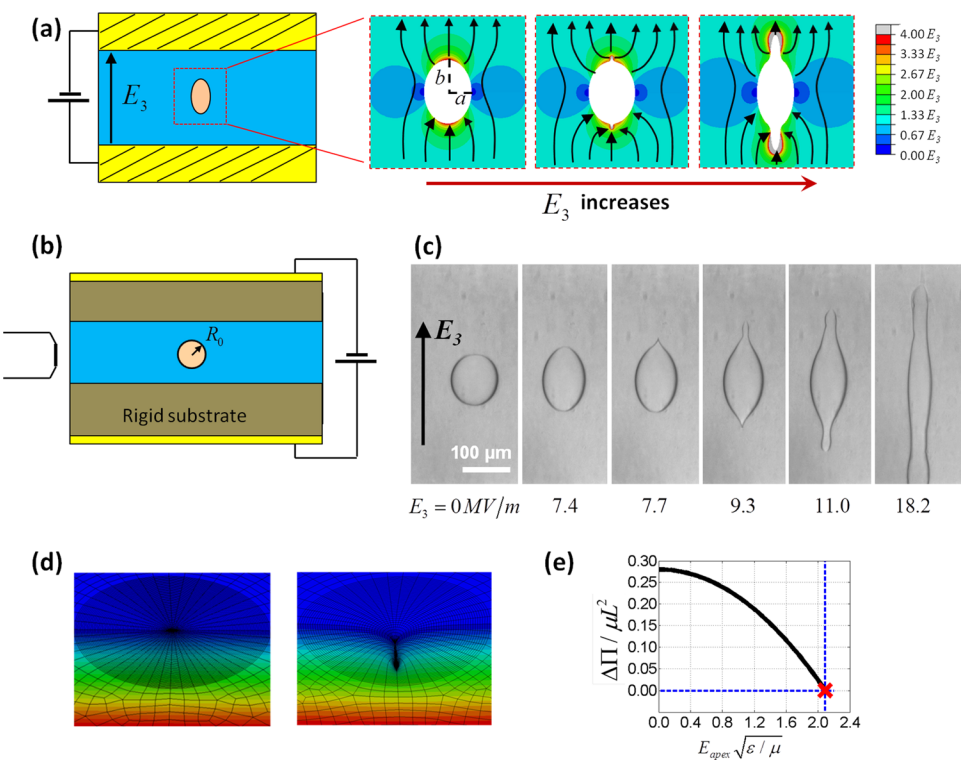

FIG. 7. Mode III, electro-cavitation instability in two-side-constrained soft-dielectric films with defects: (a) schematics of the deformation and electro-cavitation instability, (b) experimental setup for observation of the deformation and instability, (c) optical microscopic images of the process of deformation and instability, and (d) and (e) theoretical prediction of the onset of the electro-cavitation. The counters and arrows in (a) represent the magnitude and directions of the electric field in the soft dielectric. The counters in (d) represent electrical potential in the soft dielectric at the flat and sharp-tip states. The difference of Gibbs free energy of the two states, $\Delta\Pi$, is plotted as a function of the electric field at the apex of the drop, E_{apex}, in (e). Once the difference reaches zero, the electro-cavitation instability sets in. Reprinted with permission from Wang *et al.*, Nat. Commun. **3**, 1157 (2012). Copyright 2012 Nature Publishing Group.[72]

which can be calculated with Eq. (31) with H_s as the total thickness of the two insulating films. In this way, the deformation and instability of the drops can be observed using optical microscope lenses in directions along and normal to the applied electric field (Fig. 7(b)).

2. Theoretical analysis

The electric field in the soft dielectric around the conductive drop is inhomogeneous (Fig. 7(a)). Along the applied electric field, the two apexes of the drop have the highest field $E_{apex} = 3E_3$,[59] where E_3 is the applied field calculated by Eq. (31). From Eq. (25), the true stress in the soft dielectric at the apexes of the drop can be expressed as

$$\sigma_1 = \sigma_2 = -\varepsilon E_{apex}^2, \tag{35a}$$

$$\sigma_3 = 0, \tag{35b}$$

where the hydrostatic pressure in the water drop, which is equal to $-\sigma_3$, is assumed to be zero. Therefore, the magnified electric field at the apexes of the drop E_{apex} induces in-plane compressive stresses. The stresses gradually deform the drop into a spheroid shape (Figs. 7(a) and 7(c)). The local electric field at the apex of the conductive spheroid is further magnified and can be calculated as[130–132]

$$E_{apex} = E_3 \frac{(b^2 - a^2)^{3/2}}{a^2\left[b\coth^{-1}\left(b/\sqrt{b^2-a^2}\right) - \sqrt{b^2-a^2}\right]}, \tag{36}$$

where b and a are the long and short axes of the spheroid drop. The experiment of Wang *et al.* shows that $b/a \approx 1.33$ right before the formation of the tip and therefore $E_{apex} \approx 3.83E_3$ from Eq. (36). To calculate the critical electric field for formation of the sharp tip, an axisymmetric finite-element model of the soft dielectric at the apex of the drop is constructed (Fig. 7(d)).[72] Since the size of the tip at initiation is much smaller than the radius of curvature of the apex, the apex can be regarded as a flat surface under an electric field E_{apex}. The surface is also under a biaxial stretch of 1.13 to account for the deformation of the drop.[72] Using the finite-element model, the Gibbs free energies of the soft dielectric at flat and sharp-tip states can be compared as a function of E_{apex}. When the free energy difference reaches zero, the sharp tip forms. We find that the critical E_{apex} for a sharp tip to form is $2.11\sqrt{\mu/\varepsilon}$. Considering $E_{apex} \approx 3.83E$, the critical applied electric field for the electro-cavitation instability can be calculated to be $E_{3c} \approx 0.55\sqrt{\mu/\varepsilon}$, which is much lower than the critical fields for pull-in and electro-creasing instabilities (Table IV).

In addition, if multiple drops close to one another coexist in a soft dielectric film, the electric field between them can be enhanced much higher than the value predicted by Eq. (36). As a result, the critical electric field for electro-cavitation instability in soft dielectrics with multiple drops may be significantly lower than that for a single drop in the same soft dielectric.[72]

V. SUPPRESSING ELECTROMECHANICAL INSTABILITIES

A. Enhancing actuation strain by suppressing pull-in instability

As discussed in Sec. IV A, soft dielectric films coated with compliant electrodes thin down under applied voltages, an actuation mechanism that has been widely used by various types of soft-dielectric actuators. However, the pull-in instability occurs in neo-Hookean ideal dielectrics at an area actuation strain ~40% (i.e., $\lambda_{3c} \approx 0.63$), which can subsequently lead to electrical breakdown. The breakdown voltage of the soft-dielectric film can be expressed as

$$\Phi_B = E_B H \lambda_3, \tag{37}$$

where E_B is the breakdown true electric field of the dielectric. Assuming E_B to be a constant, the breakdown voltage can be plotted as a linear function of λ_3 as shown in Fig. 8(b). If the curve of Φ vs. λ_3 for a soft dielectric reaches the region above the line of Φ_B vs. λ_3, electrical breakdown occurs in the dielectric. Once the pull-in instability occurs in a neo-Hookean ideal dielectric, the dielectric film thins down drastically at a critical voltage, and crosses the line of Φ_B vs. λ_3, resulting in electrical breakdown (Fig. 8(b)).

TABLE IV. Summary of three generic models of deformation and instabilities in soft dielectrics.

	Mechanical constraint	Critical electric field	Phenomenon	Applications by suppressing instability	Applications by harnessing instability
Mode I: pull-in	No constraint	$E_{3c} \approx 1.1\sqrt{\mu/\varepsilon}$; $\tilde{E}_{3c} \approx 0.69\sqrt{\mu/\varepsilon}$	Thinning	• Enhance actuation strain of actuators • Enhance energy density of capacitors and insulators	• Achieve giant actuation strain
Mode II: electro-creasing to cratering	Constraint on one surface	$E_{3c} = \tilde{E}_{3c} \approx 1.03\sqrt{\mu/\varepsilon}$	Forming creases and craters	• Enhance energy density of capacitors and insulators	• Dynamic surface patterning •Active antifouling
Mode III: electro-cavitation	Constraint on both surfaces (a water drop encapsulated)	$E_{3c} = \tilde{E}_{3c} \approx 0.55\sqrt{\mu/\varepsilon}$	Forming sharp tips on drop	• Enhance energy density of capacitors and insulators	• To be explored

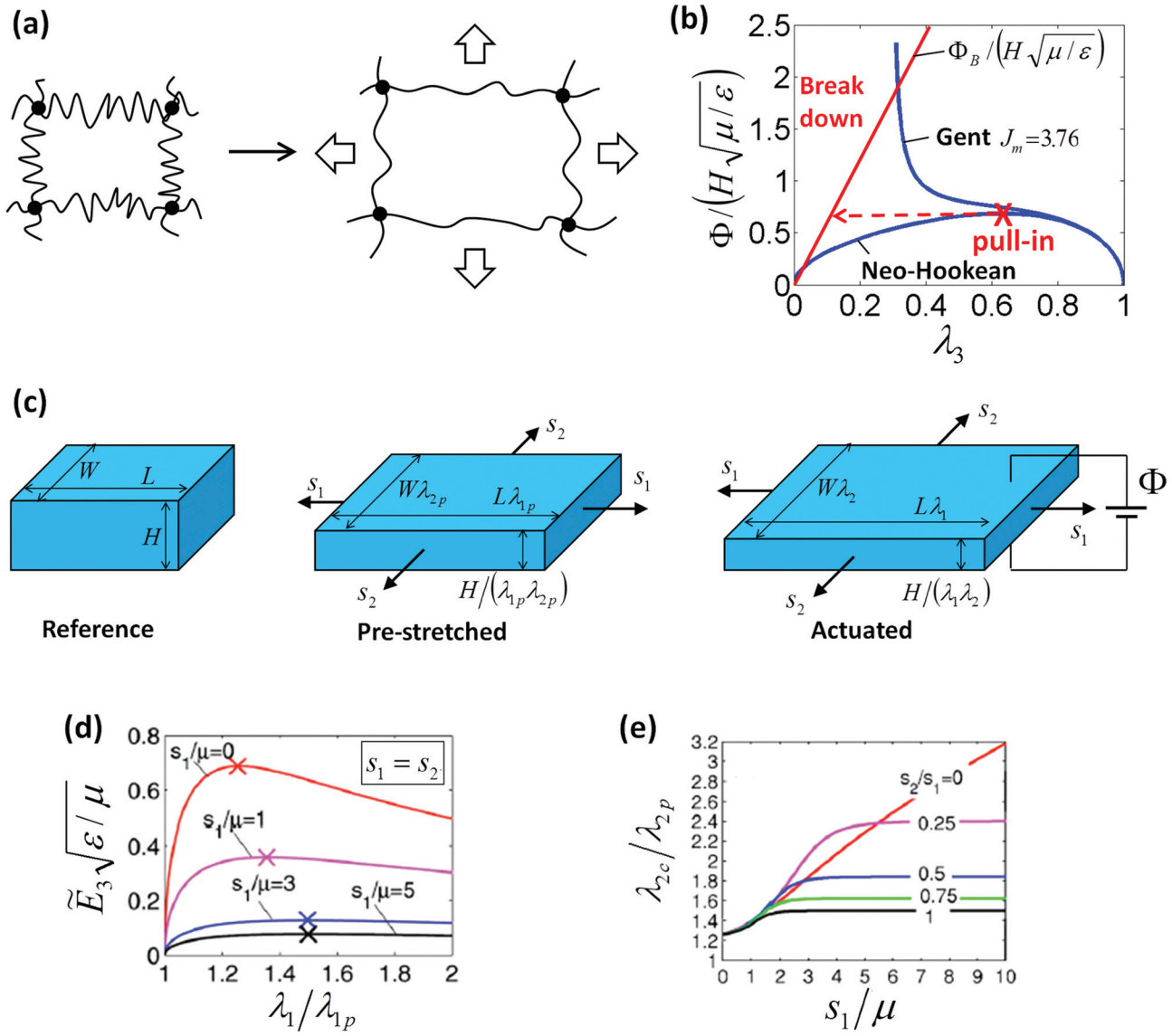

FIG. 8. Prevention and delay of the pull-in instability can increase actuation strains of unconstrained soft-dielectric films: (a) schematics of the method to use stiffening polymers to prevent the pull-in instability, and (b) the actuation stretch, λ_3, of non-stiffening neo-Hookean polymer and stiffening polymer as functions of the applied voltage, Φ. Polymers with sufficiently stiffening properties can prevent the pull-in instability to enhance actuation strain. (c) Schematics of the method to use mechanical pre-stretches to delay the pull-in instability, (d) the actuation stretch, λ_1/λ_{1p}, of pre-stretched neo-Hookean polymer as functions of the applied voltage, Φ, and (e) the critical stretch for pull-in instability, $\lambda_{2c}/\lambda_{2p}$, as functions of pre-stretch, s_1 and s_2 [Reprinted with permission from X. H. Zhao and Z. G. Suo, Appl. Phys. Lett. **91**, 061921 (2007). Copyright 2007 American Physical Society[69]]. Mechanical pre-stretches can significantly delay the pull-in instability to enhance actuation strain.

From Fig. 8(b), it is evident that the pull-in instability indeed limits the area actuation strain of neo-Hookean ideal dielectrics to ~40%. In order to increase the actuation strain to higher values (e.g., 100%), one needs to suppress or significantly delay the occurrence of pull-in instability in soft dielectrics. In development of dielectric-elastomer actuators, two methods have been widely used to suppress or delay the pull-in instability for enhancing actuation strains.

1. Soft dielectrics with stiffening properties to suppress pull-in instability

When the elastic stress in an unconstrained neo-Hookean ideal-dielectric film cannot resist the Maxwell stress from the electric field, the pull-in instability occurs in the film. Neo-Hookean elastomers assume that their polymer chains have infinite number of effective monomers (or Kuhn segments),[133–135] so that the end-to-end distance of stretched polymer chains is much smaller than the extension limit of the chains. Therefore, neo-Hookean elastomers do not stiffen under very large deformation. On the other hand, since real elastomers generally have a finite number of effective monomers, they can stiffen significantly when the end-to-end distance of stretched polymer chains approaches their extension limit (Fig. 8(a)). If a soft dielectric stiffens sufficiently before its area actuation strain reaches ~40%, the pull-in instability can be potentially suppressed. While many hyperelastic models can account for the stiffening effect of elastomers,[136] the Gent model is used here as an example. The nominal Helmholtz free energy density of Gent elastomer can be expressed as

$$\tilde{W}_M = -\frac{\mu J_m}{2}\ln\left[1-\frac{\text{trace}(\mathbf{F}^T\mathbf{F})-3}{J_m}\right]-p(J-1), \quad (38)$$

where $J_m > 0$ is a non-dimensional parameter that characterizes the extension limit of polymer chains. When J_m approaches infinite, Eq. (38) recovers the neo-Hookean model. By adding the free energy of polarization, the nominal Helmholtz free energy density of an ideal dielectric film that follows the Gent model can be expressed as

$$\tilde{W} = -\frac{\mu J_m}{2}\ln\left(1-\frac{\lambda_3^2+2\lambda_3^{-1}-3}{J_m}\right)+\frac{\lambda_3^2\tilde{D}_3^2}{2\varepsilon}. \quad (39)$$

By substituting Eq. (39) into Eq. (21), the nominal stress and nominal electric field can be calculated as

$$s_3 = \frac{\mu J_m}{J_m-\lambda_3^2-2\lambda_3^{-1}+3}\left(\lambda_3-\lambda_3^{-2}\right)+\frac{\lambda_3\tilde{D}_3^2}{\varepsilon}, \quad (40a)$$

$$\tilde{E}_3 = \frac{\lambda_3^2\tilde{D}_3}{\varepsilon}. \quad (40b)$$

With $s_3 = 0$, we can obtain the relation between the applied voltage and the deformation as

$$\frac{\Phi}{H} = \tilde{E}_3 = \sqrt{\frac{\mu J_m}{\varepsilon\left(J_m-\lambda_3^2-2\lambda_3^{-1}+3\right)}\left(\lambda_3-\lambda_3^4\right)}. \quad (41)$$

Furthermore, the Hessian matrix can be calculated as

$$\mathbf{H} = \begin{bmatrix} \dfrac{\mu J_m\left(1+2\lambda_3^{-3}\right)}{J_m-\lambda_3^2-2\lambda_3^{-1}+3}+\dfrac{2\mu J_m\left(\lambda_3-\lambda_3^{-2}\right)^2}{\left(J_m-\lambda_3^2-2\lambda_3^{-1}+3\right)^2}+\dfrac{\tilde{D}_3^2}{\varepsilon} & \dfrac{2\lambda_3\tilde{D}_3}{\varepsilon} \\ \dfrac{2\lambda_3\tilde{D}_3}{\varepsilon} & \dfrac{\lambda_3^2}{\varepsilon} \end{bmatrix}. \quad (42)$$

Based on Eqs. (41) and (42), we can calculate that the relation of $\tilde{E}_3$ vs. λ_3 will be monotonic and $\det\mathbf{H} > 0$ for all admissible values of λ_3, when the stiffening parameter J_m is less than 7.34. Therefore, soft dielectrics that stiffen sufficiently under deformation can indeed prevent the pull-in instability (e.g., $J_m = 3.76$ in Fig. 8(b)).

Along with the development of theories for preventing pull-in instability,[7,68,137,138] various types of dielectric elastomers with stiffening properties have been fabricated to prevent the pull-in instability and enhance actuation strain.[139–143] For example, in order to control the stiffening properties of soft dielectrics, Ha *et al.* interpenetrated two polymer networks,[139,141] Shankar *et al.* used nanostructured polymers,[140] and Jang *et al.* synthesized dielectric elastomers based on triblock copolymers.[143] As a result, area actuation strains over 300% have been achieved, significantly higher than the critical strain of pull-in instability.

2. Mechanical pre-stretches to delay pull-in instability

Besides elastomers with steep stiffening properties, mechanical pre-stretches on soft dielectrics have also been used to delay the pull-in instability and enhance actuation strains. The pre-stretches can be applied on soft-dielectric films in different ways, such as uniaxially stretching a strip, biaxially stretching a circular piece, or blowing a balloon of soft dielectrics.[17,76,139,144] Without loss of generality, let us consider a soft-dielectric film under two in-plane nominal pre-stresses, s_1 and s_2, respectively (Fig. 8(c)). The pre-stresses deform the soft-dielectric film by stretches of λ_{1p} and λ_{2p} along two in-plane directions. An applied voltage further deforms the soft-dielectric film to stretches of λ_1 and λ_2 (Fig. 8(c)). The actuation stretches in the two in-plane directions can be defined as λ_1/λ_{1p} and λ_2/λ_{2p}, respectively. Assuming the soft dielectric follows incompressible neo-Hookean ideal-dielectric law, we can express its nominal Helmholtz free energy density as[69]

$$\tilde{W} = \frac{1}{2}\mu\left(\lambda_1^2+\lambda_2^2+\lambda_1^{-2}\lambda_2^{-2}-3\right)+\frac{\tilde{D}_3^2}{2\varepsilon\lambda_1^2\lambda_2^2}. \quad (43)$$

Substituting Eq. (43) into Eq. (21), we have

$$s_1 = \mu\left(\lambda_1-\lambda_1^{-3}\lambda_2^{-2}\right)-\frac{\tilde{D}_3^2}{\varepsilon}\lambda_1^{-3}\lambda_2^{-2}, \quad (44a)$$

$$s_2 = \mu\left(\lambda_2-\lambda_2^{-3}\lambda_1^{-2}\right)-\frac{\tilde{D}_3^2}{\varepsilon}\lambda_2^{-3}\lambda_1^{-2}, \quad (44b)$$

$$\tilde{E}_3 = \frac{\tilde{D}_3}{\varepsilon}\lambda_1^{-2}\lambda_2^{-2}. \quad (44c)$$

The Hessian matrix becomes[69]

$$\mathbf{H} = \begin{bmatrix} \mu\left(1+3\lambda_1^{-4}\lambda_2^{-2}\right)+\frac{3\tilde{D}_3^2}{\varepsilon}\lambda_1^{-4}\lambda_2^{-2} & 2\mu\lambda_1^{-3}\lambda_2^{-3}+\frac{2\tilde{D}_3^2}{\varepsilon}\lambda_1^{-3}\lambda_2^{-3} & -\frac{2\tilde{D}_3}{\varepsilon}\lambda_1^{-3}\lambda_2^{-2} \\ 2\mu\lambda_1^{-3}\lambda_2^{-3}+\frac{2\tilde{D}_3^2}{\varepsilon}\lambda_1^{-3}\lambda_2^{-3} & \mu\left(1+3\lambda_2^{-4}\lambda_1^{-2}\right)+\frac{3\tilde{D}_3^2}{\varepsilon}\lambda_2^{-4}\lambda_1^{-2} & -\frac{2\tilde{D}_3}{\varepsilon}\lambda_2^{-3}\lambda_1^{-2} \\ -\frac{2\tilde{D}_3}{\varepsilon}\lambda_1^{-3}\lambda_2^{-2} & -\frac{2\tilde{D}_3}{\varepsilon}\lambda_2^{-3}\lambda_1^{-2} & \frac{1}{\varepsilon}\lambda_1^{-2}\lambda_2^{-2} \end{bmatrix}. \quad (45)$$

In the special case when the elastomer is under equi-biaxial stresses (i.e., $s_1 = s_2$ and thus $\lambda_1 = \lambda_2$), Eq. (44) gives

$$\frac{\Phi}{H} = \tilde{E}_3 = \sqrt{\frac{\mu\lambda_1^{-2} - \mu\lambda_1^{-8} - s_1\lambda_1^{-3}}{\varepsilon}}. \quad (46)$$

In Fig. 8(d), we plot the actuation stretch λ_1/λ_{1p} as a function of applied voltage for various levels of equi-biaxial stresses. The critical points for the pull-instability by solving Eq. (45) are also indicated on the curves. From Fig. 8(d), it can be seen that the equi-biaxial stresses indeed delay the critical actuation stretch for pull-in from ~1.26 to ~1.5. The critical actuation stretches for various unequal biaxial stresses are further summarized in Fig. 8(e). It can be seen that uniaxial pre-stress in one direction (e.g., s_1) can greatly enhance the critical actuation stretch in the other direction (e.g., λ_2/λ_{2p}).

Pelrine *et al.* first demonstrated that dielectric elastomers can achieve actuation strains over 100%, by uniaxially or biaxially pre-stretching elastomer films such as silicone rubber and VHB prior to actuation.[17] Thereafter, various experimental and theoretical studies were carried out to investigate the effects of pre-stretches on enhancing actuation strains in various types of dielectric-elastomer actuators including ring actuator,[108,145] spring-roll actuator,[24,146] balloon actuator,[76,147,148] folded actuator,[149] helical actuator,[150] cone actuator,[151,152] fiber actuator,[153] and bi-stable actuator.[154]

In addition, since mechanical pre-stretches on elastomers can tune the degree of their stiffening, a combination of the use of stiffening elastomers and pre-stretches is particularly effective in suppressing or delaying the pull-in instability.[68,137] In fact, many existing dielectric-elastomer actuators rely on a combination of both methods to achieve large actuation strains. Moreover, charge-controlled operation has been recently explored to suppress the pull-in instability in electrode-free dielectric elastomers, since the deposited charges cannot freely redistribute.[73–75]

B. Enhancing electrical energy density by suppressing all modes of instabilities

Electrical energy density is a critical performance parameter for dielectric capacitors and insulators. The maximum electrical energy density for an ideal dielectric can be expressed as

$$u_{\max} = \varepsilon E_B^2/2, \quad (47)$$

where E_B is the breakdown true electric field of the dielectric. If the electrical breakdown is caused by pull-in, electro-creasing, or electro-cavitation instability, the maximum energy density can be calculated as

$$u_{\max} = Z\mu, \quad (48)$$

where the non-dimensional parameter $Z \approx 0.61$ for pull-in, 0.53 for electro-creasing, and 0.15 for electro-cavitation instability (Table IV). Since the moduli of soft dielectrics are generally less than 1 MPa, their maximum electrical energy density, if limited by the instabilities, usually cannot exceeds 1 J cm^{-3}.

In order to significantly enhance electrical energy density of soft dielectrics, all modes of electromechanical instabilities that cause breakdown need to be suppressed.[9,11,48,155–157] Zhang *et al.* tested the breakdown fields and energy densities of soft dielectrics subject to different types of mechanical constraints by using either carbon grease or carbon epoxy as electrodes.[48] The carbon grease deforms freely with the dielectric, while a thick layer of carbon epoxy can mechanically constrain the surface of the film. Three types of mechanical constraints were employed: unconstrained (Fig. 4(a)), one-side-constrained (Fig. 4(b)), and two-side-constrained (Fig. 4(c)). As expected, the breakdown fields for unconstrained and one-side-constrained films are significantly lower than that of two-side-constrained film (Fig. 9(a)). The results proved that proper mechanical constraints can suppress the pull-in and electro-creasing instabilities and, therefore, greatly enhance breakdown fields and electrical energy densities of soft dielectrics.

In addition, Wang *et al.* measured the breakdown fields of two-side-constrained soft-dielectric films that encapsulate water drops and air bubbles.[72] Despite the mechanical constraints, defects can significantly reduce breakdown fields of soft dielectrics, potentially due to the electro-cavitation instability (Fig. 9(b)). Based on these studies, we can see that a simple yet effective method for enhancing electrical energy densities of soft dielectrics is to suppress all modes of electromechanical instabilities by eliminating defects in the dielectrics and properly constraining the dielectrics with rigid components.[48,72]

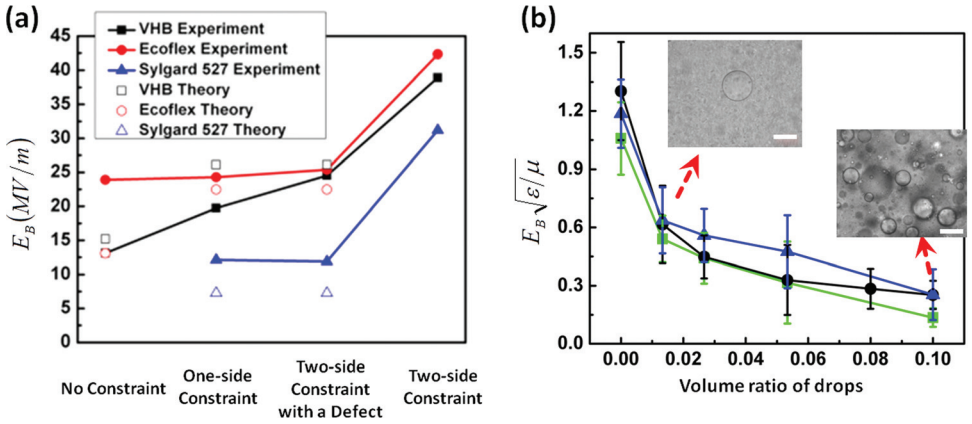

FIG. 9. Prevention of all modes of instabilities can enhance the breakdown field and energy density of soft-dielectric films: (a) the breakdown fields of two-side-constrained films are much higher than unconstrained and one-side-constrained films. Reprinted with permission from Zhang *et al*., Appl. Phys. Lett. **99**, 171906 (2011). Copyright 2011 AIP Publishing.[48] (b) Elimination of defects can significantly enhance breakdown fields of soft dielectrics. Reprinted with permission from Wang *et al*. Nat. Commun. **3**, 1157 (2012). Copyright 2013 Nature Publishing Group.[72]

VI. HARNESSING ELECTROMECHANICAL INSTABILITIES FOR APPLICATIONS

Electromechanical instabilities are traditionally regarded as detrimental failure modes of soft dielectrics, and intensive efforts have been devoted to the prevention of instabilities.[9] Recent paradigm-shift discoveries in the field, however, show that transformative applications and extraordinary functions can be achieved through accurate prediction and judicious control of electromechanical instabilities in soft dielectrics. This section will summarize recent progress in harnessing large deformation and instabilities of soft dielectrics for applications and functions.

A. Harnessing pull-in instability for giant actuation strain

Soft dielectric films without mechanical constraints (i.e., compliant electrodes on both surfaces) may be susceptible to pull-in instability or not, dependent on their stiffening properties. While the pull-in instability sets in neo-Hookean ideal dielectrics (i.e., no stiffening) and induces subsequent electrical breakdown (Fig. 8(b)), soft dielectrics with sufficiently rapid stiffening properties can prevent the pull-in instability (i.e., $J_m < 7.34$ in Fig. 8(b)). In addition to the above two scenarios, Zhao and Suo proposed a third scenario in which the pull-in instability is harnessed to give giant actuation strain of dielectric elastomers under voltages (Fig. 10).[7]

As illustrated in Fig. 10(a), soft dielectrics with stiffening properties less rapid than J_m of 7.34 will undergo the pull-in instability. During the instability, the soft dielectric can drastically deform to a much thinner state and stabilize due to the stiffening of the polymer.[68,158] If the stable state is in the region below the line of Φ_B vs. λ_3, the electrical breakdown can be avoided, despite the occurrence of pull-in instability (e.g., $J_m = 12.4$ in Fig. 10(a)). In this way, the pull-in instability can be controlled and harnessed by using soft dielectrics with appropriate stiffening properties to achieve giant deformation of actuation (e.g., $\lambda_3 < 0.2$ in Fig. 10(a)). By harnessing the pull-in instability, Keplinger *et al*.[50] and Li *et al*.[159] achieved impressive area-actuation strain over 1600% with balloon-shape actuators of dielectric elastomers (Fig. 10(b)).

B. Harnessing electro-creasing to cratering instability

As discussed in Sec. IV B, in order to observe the electro-creasing instability, soft dielectric films have been

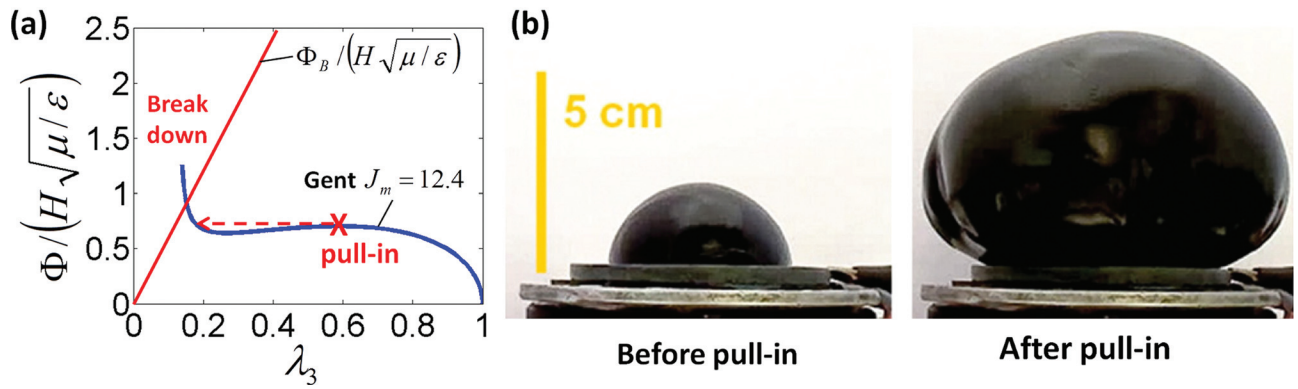

FIG. 10. By harnessing the pull-in instability, soft dielectrics can achieve giant actuation strains: (a) the actuation stretch λ_3 of a properly stiffening polymer as a function of voltage, Φ. The polymer can survive the pull-in instability without electrical breakdown and stabilize at a thinner state to achieve giant actuation strain. (b) Experimental observation of a balloon-shape dielectric-elastomer actuator to achieve actuation strain over 1600% by harnessing the pull-in instability. Reprinted with permission from Keplinger *et al*., Soft Matter **8**, 285–288 (2012). Copyright 2012 Royal Society of Chemistry.[50]

sandwiched between complaint electrodes and rigid dielectric substrates, which prevent electrical breakdown of the soft dielectrics (Fig. 6(b)). The same method can be employed to integrate soft dielectrics into structures and exploit the electro-creasing and electro-cratering instabilities for transformative applications.

1. Dynamic surface patterning

Topographical patterns on polymer surfaces are of fundamental importance in material science, physics, chemistry, and biology. While surface patterns generated with conventional methods such as imprinting and lithography are generally static, i.e., fixed in their final states, surface patterns capable of dynamic and on-demand tunability are highly desirable for various applications such as on-demand superhydrophobicity,[160] tunable adhesion,[161,162] switchable optics,[163] controlled drug release,[164] anti-fouling coatings,[165] and transfer printing.[166]

Wang *et al*. recently discovered that the electro-creasing and cratering instability in soft dielectrics can be harnessed to dynamically control surface patterning with voltages.[51] Large-area films of soft dielectrics (e.g., silicone elastomer) and rigid dielectrics (e.g., Kapton) and metal foils were laminated together as illustrated in Fig. 11(a). The top surface of the soft dielectric was further coated with a complaint electrode (e.g., NaCl solution). Electrical voltages applied between the metal foil and the compliant electrode can induce electro-creasing to cratering instabilities, giving dynamic surface patterns.

In addition, the soft-dielectric films can also be uniaxially pre-stretched, prior to bonding on rigid dielectric substrates. The pre-stretch induces a tensile stress, which tends to align the creases and craters along the pre-stretched direction. Using the pre-stretch ratio λ_p and applied electric field E_3 as two control parameters, Wang *et al*. constructed a phase diagram (Fig. 11(b)) that can predict the generation of various surface patterns including randomly oriented creases and craters, and aligned creases, craters, and lines (Fig. 11(c)).

Moreover, since adjacent creases and craters in a soft-dielectric film interacts with each other over a length scale of the film thickness, the wavelength of surface patterns scales with the film thickness. The experiments of Wang *et al*. show that the wavelengths for aligned and randomly oriented patterns can be expressed as

$$l_{aligned} \approx 1.0H, \tag{49a}$$

$$l_{random} \approx 1.5H. \tag{49b}$$

Based on the phase diagram (Fig. 11(b)) and Eq. (49), one can design surface patterns with various shapes and feature sizes on demand by simply tuning film thickness, pre-stretch, and applied voltage in a controlled manner (e.g., Figs. 11(c) and 11(d)).

2. Active control of biofouling

Biofouling, the accumulation of unwanted biological organisms on submerged or implanted surfaces, is a ubiquitous problem in maritime operations, medicines, food industries, and biotechnology.[167–169] Development of environmentally friendly and biocompatible surfaces that can effectively manage biofouling has been an extremely challenging task across multiple disciplines. While existing anti-fouling surfaces are mostly static, many biological surfaces can effectively clean themselves through active deformation and motion.[170–174] For example, cilia on the surfaces of respiratory tracts constantly sweep out inhaled foreign particles.[171–173]

Inspired by biological surfaces that use active deformation for antifouling, Shivapooja *et al*. harnessed the electro-cratering instability that deforms the surface of a soft-dielectric film to detach biofouling adhered on it.[52] They bonded a soft-dielectric film (e.g., silicone rubber), a

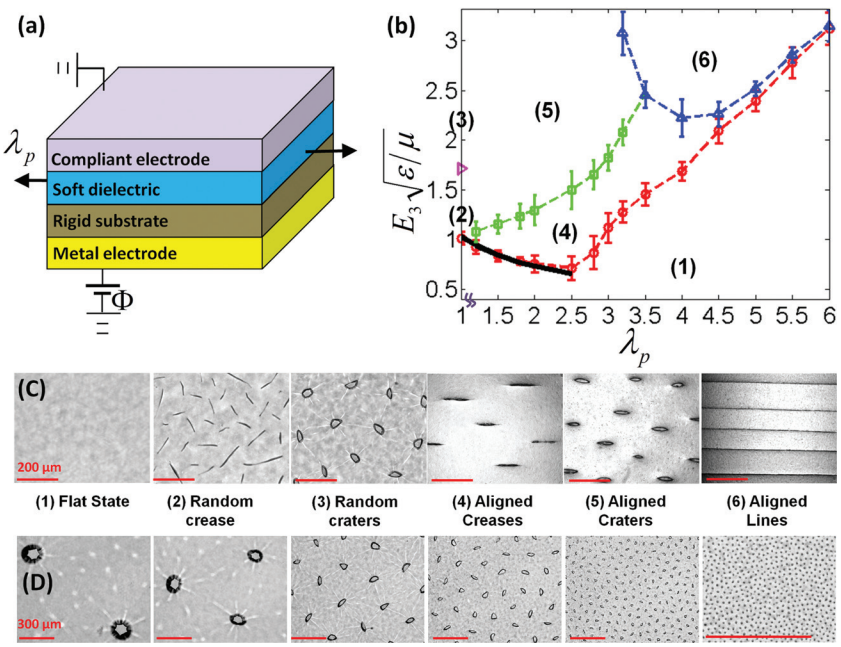

FIG. 11. By harnessing the electro-creasing to cratering instability, soft dielectrics can give dynamic surface patterning: (a) schematic illustration of the experimental setup. (b) A phase diagram for the transition of the dynamic surface patterns. The pattern transition is controlled by two parameters, the applied electric field E_3 and the uniaxial pre-stretch ratio λ_p. (c) Optical microscope images of various patterns ranging from randomly oriented creases and craters to aligned creases, craters, and lines. (d) Optical microscope images of crater patterns with various wavelengths ranging from millimeter to micrometer. The scale bars are 300 μm. Reprinted with permission from Wang *et al*., Adv. Mater. **25**, 1430 (2012). Copyright 2012 Wiley-VCH Verlag GmbH & Co. KGaA.[52]

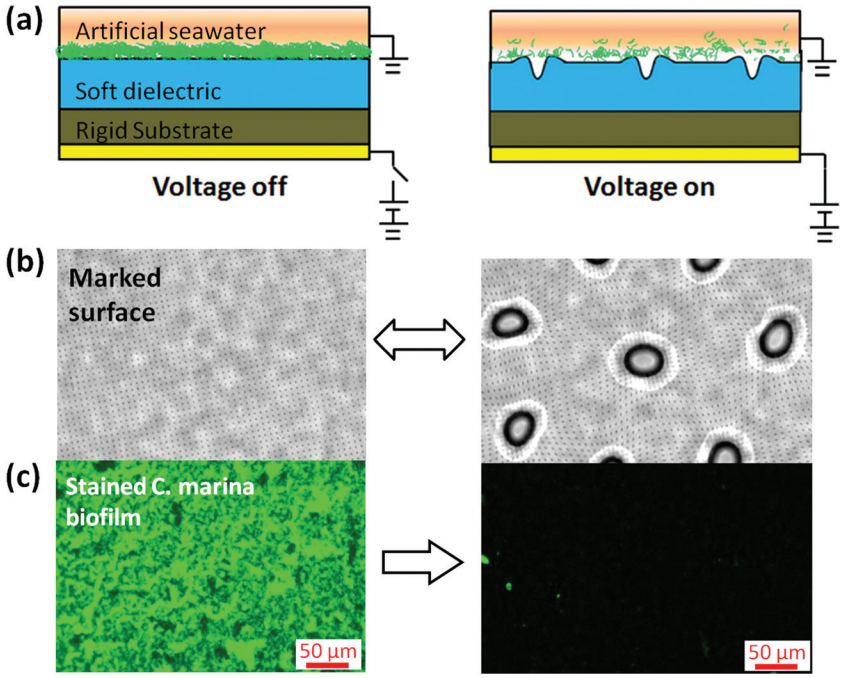

FIG. 12. By harnessing the electro-creasing to cratering instability, soft dielectrics can give active control of biofouling: (a) schematic illustration of the experimental setup. (b) The applied electric field can induce significant deformation of the soft dielectric as given by the contours of the maximum principal strain. (c) The deformation detaches over 95% of a biofilm (*Cobetia marina*) adhered to the surface of the soft dielectric. Reprinted with permission from Shivapooja *et al.*, Adv. Mater. **25**, 1430 (2013). Copyright 2013 Wiley-VCH Verlag GmbH & Co. KGaA.[52]

rigid dielectric film (e.g., Kapton), and a metal foil together to form a trilayer laminate (Fig. 12(a)). The soft-dielectric surface was immersed in artificial seawater to allow biofouling such as bacterial film to accumulate on it. Thereafter, a direct-current voltage was applied on the metal foil, while the artificial seawater was grounded (Fig. 12(a)). When the electric field in the soft dielectric reached a critical value, the electro-cratering instability sets in, significantly deforming the surface of the soft dielectric (e.g., strain over 20% in Fig. 12(b)). As shown in Fig. 12(c), the deformation can detach over 95% of the bacterial film adhered on the surface. The new paradigm of harnessing surface deformation and instabilities of soft dielectrics has the potential to be implemented in various applications for effective and active control of biofouling.

VII. FUTURE DIRECTIONS

Widely used as insulators, capacitors, and transducers in daily life, soft dielectrics based on polymers and polymeric gels play important roles in modern electrified society. Compared with conventional hard dielectrics, soft dielectrics possess a unique set of merits including low cost, light weight, mechanical flexibility, fast charging rate, low-temperature fabrication, and easy processing. The emergence of new electronic, robotic, biomedical, and electrical-energy-storage technologies[175–179] is imposing even higher requirements on the attributes of next-generation soft dielectrics for a broad spectrum of applications. For example, it is desirable for soft dielectrics used as insulators and capacitors to have high energy density, high working temperature, and high reliability, while soft-dielectric transducers generally need to reach high actuation stress and strain, fast response, high energy density and efficiency, and high reliability. In order to achieve the unprecedented set of properties and merits, soft dielectrics with new compositions and new nano-, micro-, and meso-structures are being intensively developed and explored. Consequently, the research on large deformation and instabilities of soft dielectrics is rapidly evolving toward new directions to account for the properties and functions of new materials and structures.

A. Non-ideal dielectric properties of soft dielectrics

Most of existing models for soft dielectrics follow the ideal-dielectric law, which assumes the dielectric's polarization property is fully characterized by the dielectric constant, unaffected by applied electric field or deformation. Next-generation capacitors, insulators, and transducers generally require soft dielectrics to sustain high electric fields and/or large deformation, so as to achieve high energy density and/or high actuation strain. Subject to high fields and large deformation, however, the polarization of soft dielectrics can drastically deviate from the ideal-dielectric model, giving non-ideal behaviors such as electrostriction,[180–186] polarization saturation,[182,187,188] and leakage current.[189] While it has been shown that electrostriction and polarization saturation can delay pull-in instabilities of soft dielectrics,[182–185,187] the effects of non-ideal dielectric properties on deformation and instabilities of soft dielectrics have not been systematically understood. One future research direction in the field is to fundamentally understand and judiciously control (e.g., prevent or harness) the non-ideal dielectric properties of soft dielectrics.

B. Viscoelasticity of soft dielectrics

Soft dielectrics are usually taken as elastic or hyperelastic materials in existing studies. However, subjected to electrical and/or mechanical loads, many elastomer-based soft dielectrics indeed undergo time-dependent viscoelastic deformation,[128,190–195] which needs to be characterized by non-equilibrium thermodynamic models.[193] While it has been shown that viscoelasticity of soft dielectrics can delay

the occurrence of pull-in instability, the effects of viscoelasticity on electro-creasing, electro-cratering, and electro-cavitation instabilities have not been explored.[93,142–145] In addition, although the viscoelasticity may be used to control deformation and instabilities of soft dielectrics, its dissipative nature also reduces the energy efficiency of soft-dielectric transducers.[192,193,196] Therefore, it is an important task to understand the effects of viscoelastic properties of soft dielectrics on their deformation, instabilities, and other performance in various applications.

C. Fracture and fatigue of soft dielectrics

Electric fields and mechanical forces applied on soft dielectrics can lead to fracture and fatigue of the dielectrics.[71,72] As failure modes that are distinctly different from instabilities and breakdown, fracture and fatigue have been extensively studied in hard dielectrics such as piezoelectric ceramics and rigid polymers.[97,197] Wang *et al*. recently observed crack propagation in soft dielectrics undergoing the electro-cratering and electro-cavitation instabilities.[71,72] However, fracture and fatigue of soft dielectrics, which are usually coupled with large deformation and instabilities, have not been quantitatively explored or understood. Such an understanding will have significant impacts on both fundamental knowledge of physics and mechanics and long-term reliability of soft dielectrics.

D. Soft-dielectric composites

In order to achieve novel properties and functions, new types of soft dielectrics are being intensively developed by integrating multiple components together to form composites. Examples include interpenetration of polymer networks,[139,141,198] polymer blends,[199–203] incorporation of high-permittivity particles[200,204–213] or cavities,[72,214] layered structures,[71,215–221] and fiber reinforcement.[222–224] The nano-, micro-, and meso-structures of soft-dielectric composites can be rationally designed and fabricated for certain desirable properties such as high dielectric constants or high energy density. On the other hand, such designed structures may lead to unexpected modes of deformation and instabilities of soft-dielectric composites under voltages. A systematic understanding on the relations between the structures and deformation and instabilities of soft-dielectric composites is of imminent importance to their design and applications but still not available.

E. Computational models of soft dielectrics

Computational models are of critical importance to the understanding of deformation and instabilities of soft dielectrics and the design of soft-dielectric devices. Most of existing computational models of soft dielectrics are based on finite element method,[76,108,109,145,225–230] which is able to calculate the coupled electromechanical fields and large deformation of soft dielectrics. Some of the computational models can also simulate time-dependent behaviors such as viscoelastic deformation[128,231] and dynamic response[76,200,232–236] of soft dielectrics. On the other hand, most of existing computational models assume that the soft dielectrics follow the ideal dielectric law and, therefore, cannot account for non-ideal dielectric properties such as electrostriction and polarization saturation. In addition, the capabilities of calculating instabilities, fracture, fatigue, and singular electromechanical fields still need to be implemented or significantly improved in existing computational models. For example, it is still challenging to accurately simulate the electro-creasing to cratering and electro-cavitation instabilities in soft dielectrics, not to mention crack initiation and propagation during the instabilities. The development of versatile and robust computational models that can accurately characterize various emerging properties of soft dielectrics and simulate various important phenomena will greatly facilitate the fundamental understanding and practical applications of soft dielectrics.

ACKNOWLEDGMENTS

The work was supported by NSF CAREER Award (No. CMMI-1253495), NSF Grant (No. CMMI-1200515), NSF Triangle MRSEC (No. DMR-1121107), and NIH Grant (No. UH2 TR000505).

[1]S. E. Park and T. R. Shrout, "Ultrahigh strain and piezoelectric behavior in relaxor based ferroelectric single crystals," J. Appl. Phys. **82**, 1804–1811 (1997).
[2]Y. Saito *et al*., "Lead-free piezoceramics," Nature **432**, 84–87 (2004).
[3]S. E. Park and T. R. Shrout, "Relaxor based ferroelectric single crystals for electro-mechanical actuators," Mater. Res. Innovations **1**, 20–25 (1997).
[4]Q. M. Zhang, V. Bharti, and X. Zhao, "Giant electrostriction and relaxor ferroelectric behavior in electron-irradiated poly(vinylidene fluoride-trifluoroethylene) copolymer," Science **280**, 2101–2104 (1998).
[5]Q. M. Zhang *et al*., "An all-organic composite actuator material with a high dielectric constant," Nature **419**, 284–287 (2002).
[6]R. Pelrine *et al*., "High-field deformation of elastomeric dielectrics for actuators," Mater. Sci. Eng. C: Biomimetic Supramol. Syst. **11**, 89–100 (2000).
[7]X. H. Zhao and Z. G. Suo, "Theory of dielectric elastomers capable of giant deformation of actuation," Phys. Rev. Lett. **104**, 178302 (2010).
[8]P. Brochu and Q. Pei, "Advances in dielectric elastomers for actuators and artificial muscles," Macromol. Rapid Commun. **31**, 10–36 (2010).
[9]L. A. Dissado and J. C. Fothergill, *Electrical Degradation and Breakdown in Polymers* (Peter Peregrinus Ltd., 1992), Vol. 11.
[10]Z. Suo, C. M. Kuo, D. M. Barnett, and J. R. Willis, "Fracture-mechanics for piezoelectric ceramics," J. Mech. Phys. Solids **40**, 739–765 (1992).
[11]K. H. Stark and C. G. Garton, "Electric strength of irradiated polythene," Nature **176**, 1225–1226 (1955).
[12]X. Zhou *et al*., "Electrical breakdown and ultrahigh electrical energy density in poly(vinylidene fluoride-hexafluoropropylene) copolymer," Appl. Phys. Lett. **94**, 162901 (2009).
[13]X. H. Zhao and Z. G. Suo, "Electromechanical instability in semicrystalline polymers," Appl. Phys. Lett. **95**, 031904 (2009).
[14]Q. M. Wang, X. F. Niu, Q. B. Pei, M. D. Dickey, and X. H. Zhao, "Electromechanical instabilities of thermoplastics: Theory and in situ observation," Appl. Phys. Lett. **101**, 141911 (2012).
[15]Z. B. Yu *et al*., "Large-strain, rigid-to-rigid deformation of bistable electroactive polymers," Appl. Phys. Lett. **95**, 192904 (2009).
[16]J. Y. Song, Y. Y. Wang, and C. C. Wan, "Review of gel-type polymer electrolytes for lithium-ion batteries," J. Power Sources **77**, 183–197 (1999).
[17]R. Pelrine, R. Kornbluh, Q. B. Pei, and J. Joseph, "High-speed electrically actuated elastomers with strain greater than 100%," Science **287**, 836–839 (2000).
[18]F. Carpi, S. Bauer, and D. De Rossi, "Stretching dielectric elastomer performance," Science **330**, 1759–1761 (2010).

[19]F. Carpi, D. De Rossi, R. Kornbluh, R. E. Pelrine, and P. Sommer-Larsen, *Dielectric Elastomers as Electromechanical Transducers: Fundamentals, Materials, Devices, Models and Applications of an Emerging Electroactive Polymer Technology* (Elsevier, 2011).
[20]J. F. Zang *et al.*, "Multifunctionality and control of the crumpling and unfolding of large-area grapheme," Nature Mater. **12**, 321–325 (2013).
[21]G. Kovacs, L. Duering, S. Michel, and G. Terrasi, "Stacked dielectric elastomer actuator for tensile force transmission," Sens. Actuators, A **155**, 299–307 (2009).
[22]R. Shankar, T. K. Ghosh, and R. J. Spontak, "Dielectric elastomers as next-generation polymeric actuators," Soft Matter **3**, 1116–1129 (2007).
[23]F. Carpi and D. De Rossi, "Dielectric elastomer cylindrical actuators: Electromechanical modelling and experimental evaluation," Mater. Sci. Eng. C: Biomimetic Supramol. Syst. **24**, 555–562 (2004).
[24]M. Moscardo, X. H. Zhao, Z. G. Suo, and Y. Lapusta, "On designing dielectric elastomer actuators," J. Appl. Phys. **104**, 093503 (2008).
[25]G. Kofod, W. Wirges, M. Paajanen, and S. Bauer, "Energy minimization for self-organized structure formation and actuation," Appl. Phys. Lett. **90**, 081916 (2007).
[26]M. Aschwanden and A. Stemmer, "Polymeric, electrically tunable diffraction grating based on artificial muscles," Opt. Lett. **31**, 2610–2612 (2006).
[27]E. Biddiss and T. Chau, "Dielectric elastomers as actuators for upper limb prosthetics: Challenges and opportunities," Med. Eng. Phys. **30**, 403–418 (2008).
[28]F. Carpi, G. Frediani, S. Turco, and D. De Rossi, "Bioinspired tunable lens with muscle-like electroactive elastomers," Adv. Funct. Mater. **21**, 4152–4158 (2011).
[29]S. Akbari and H. R. Shea, "Microfabrication and characterization of an array of dielectric elastomer actuators generating uniaxial strain to stretch individual cells," J. Micromech. Microeng. **22**, 045020 (2012).
[30]Z. H. Fang, C. Punckt, E. Y. Leung, H. C. Schniepp, and I. A. Aksay, "Tuning of structural color using a dielectric actuator and multifunctional compliant electrodes," Appl. Opt. **49**, 6689–6696 (2010).
[31]S. I. Son *et al.*, "Electromechanically driven variable-focus lens based on transparent dielectric elastomer," Appl. Opt. **51**, 2987–2996 (2012).
[32]S. Shian, R. M. Diebold, and D. R. Clarke, "Tunable lenses using transparent dielectric elastomer actuators," Opt. Express **21**, 8669–8676 (2013).
[33]X. Niu *et al.*, "Bistable large-strain actuation of interpenetrating polymer networks," Adv. Mater. **24**, 6513–6519 (2012).
[34]B. O'Brien *et al.*, Proc. SPIE **6524**, 652415 (2007).
[35]S. Son and N. C. Goulbourne, "Finite deformations of tubular dielectric elastomer sensors," J. Intell. Mater. Syst. Struct. **20**, 2187–2199 (2009).
[36]K. Jung, K. J. Kim, and H. R. Choi, "A self-sensing dielectric elastomer actuator," Sens. Actuators A **143**, 343–351 (2008).
[37]R. Pelrine *et al.*, Proc. SPIE **4329**, 148–156 (2001).
[38]T. McKay, B. O'Brien, E. Calius, and I. Anderson, "An integrated, self-priming dielectric elastomer generator," Appl. Phys. Lett. **97**, 062911 (2010).
[39]S. Chiba *et al.*, "Consistent ocean wave energy harvesting using electroactive polymer (dielectric elastomer) artificial muscle generators," Appl. Energy **104**, 497–502 (2013).
[40]S. J. A. Koh, X. H. Zhao, and Z. G. Suo, "Maximal energy that can be converted by a dielectric elastomer generator," Appl. Phys. Lett. **94**, 262902 (2009).
[41]T. McKay, B. O'Brien, E. Calius, and I. Anderson, "Self-priming dielectric elastomer generators," Smart Mater. Struct. **19**, 055025 (2010).
[42]R. Kaltseis *et al.*, "Method for measuring energy generation and efficiency of dielectric elastomer generators," Appl. Phys. Lett. **99**, 162904 (2011).
[43]R. D. Kornbluh *et al.*, in *Dielectric Elastomers: Stretching the Capabilities of Energy Harvesting*, edited by S. Wagner and S. Bauer (Mater. Res. Sci. Bull., 2012), Vol. 37, pp. 246–253.
[44]K. Ahnert, M. Abel, M. Kollosche, P. J. Jorgensen, and G. Kofod, "Soft capacitors for wave energy harvesting," J. Mater. Chem. **21**, 14492–14497 (2011).
[45]S. J. A. Koh, C. Keplinger, T. Li, S. Bauer, and Z. Suo, "Dielectric elastomer generators: How much energy can be converted?," IEEE/ASME Trans. Mechatron. **16**, 33–41 (2011).
[46]S. Ashley, "Artificial muscles," Sci. Am. **289**, 52–59 (2003).
[47]Z. Suo, "Theory of dielectric elastomers," Acta Mech. Solida Sin. **23**, 549–578 (2010).
[48]L. Zhang, Q. M. Wang, and X. H. Zhao, "Mechanical constraints enhance electrical energy densities of soft dielectrics," Appl. Phys. Lett. **99**, 171906 (2011).
[49]Q. M. Wang, M. Tahir, L. Zhang, and X. H. Zhao, "Electro-creasing instability in deformed polymers: Experiment and theory," Soft Matter **7**, 6583–6589 (2011).
[50]C. Keplinger, T. Li, R. Baumgartner, Z. Suo, and S. Bauer, "Harnessing snap-through instability in soft dielectrics to achieve giant voltage-triggered deformation," Soft Matter **8**, 285–288 (2012).
[51]Q. M. Wang, M. Tahir, J. F. Zang, and X. H. Zhao, "Dynamic electrostatic lithography: Multiscale on-demand patterning on large-area curved surfaces," Adv. Mater. **24**, 1947–1951 (2012).
[52]P. Shivapooja *et al.*, "Bioinspired surfaces with dynamic topography for active control of biofouling," Adv. Mater. **25**, 1430–1434 (2013).
[53]A. O'Halloran, F. O'Malley, and P. McHugh, "A review on dielectric elastomer actuators, technology, applications, and challenges," J. Appl. Phys. **104**, 071101 (2008).
[54]I. A. Anderson, T. A. Gisby, T. G. McKay, B. M. O'Brien, and E. P. Calius, "Multi-functional dielectric elastomer artificial muscles for soft and smart machines," J. Appl. Phys. **112**, 041101 (2012).
[55]Y. Bar-Cohen and Q. M. Zhang, in *Electroactive Polymer Actuators and Sensors*, edited by Z. Cheng and Q. Zhang (Mater. Res. Sci. Bull., 2008), Vol. 33, pp. 173–181.
[56]C. Lowe, X. Q. Zhang, and G. Kovacs, "Dielectric elastomers in actuator technology," Adv. Eng. Mater. **7**, 361–367 (2005).
[57]J. L. Mead, Z. Tao, and H. S. Liu, "Insulation materials for wire and cable applications," Rubber Chem. Technol. **75**, 701–712 (2002).
[58]R. A. Toupin, "The elastic dielectric," J. Rational Mech. Anal. **5**, 849–915 (1956).
[59]L. D. Landau and E. M. Lifshitz, *Electrodynamics of Continuous Media* (Pergamon, 1984).
[60]J. A. Stratton, *Electromagnetic Theory* (McGraw-Hill, 1941).
[61]A. Dorfmann and R. W. Ogden, "Nonlinear electroelasticity," Acta Mech. **174**, 167 (2005).
[62]R. M. McMeeking and C. M. Landis, "Electrostatic forces and stored energy for deformable dielectric materials," ASME Trans. J. Appl. Mech. **72**, 581–590 (2005).
[63]Z. G. Suo, X. H. Zhao, and W. H. Greene, "A nonlinear field theory of deformable dielectrics," J. Mech. Phys. Solids **56**, 467–486 (2008).
[64]A. Dorfmann and R. W. Ogden, "Nonlinear electroelastic deformations," J. Elasticity **82**, 99–127 (2006).
[65]R. W. Ogden, *Nonlinear Elastic Deformations* (Dover Publications, 1997).
[66]G. A. Holzapfel, *Nonlinear Solid Mechanics: A Continuum Approach for Engineering* (Wiley, 2000).
[67]M. E. Gurtin, E. Fried, and L. Anand, *The Mechanics and Thermodynamics of Continua* (Cambridge University Press, 2010).
[68]X. H. Zhao, W. Hong, and Z. G. Suo, "Electromechanical hysteresis and coexistent states in dielectric elastomers," Phys. Rev. B **76**, 134113 (2007).
[69]X. H. Zhao and Z. G. Suo, "Method to analyze electromechanical stability of dielectric elastomers," Appl. Phys. Lett. **91**, 061921 (2007).
[70]A. Dorfmann and R. W. Ogden, "Nonlinear electroelastostatics: Incremental equations and stability," Int. J. Eng. Sci. **48**, 1–14 (2010).
[71]Q. M. Wang, L. Zhang, and X. H. Zhao, "Creasing to cratering instability in polymers under ultrahigh electric fields," Phys. Rev. Lett. **106**, 118301 (2011).
[72]Q. M. Wang, Z. G. Suo, and X. H. Zhao, "Bursting drops in solid dielectrics caused by high voltages," Nat. Commun. **3**, 1157 (2012).
[73]C. Keplinger, M. Kaltenbrunner, N. Arnold, and S. Bauer, "Röntgen's electrode-free elastomer actuators without electromechanical pull-in instability," Proc. Natl. Acad. Sci. U. S. A. **107**, 4505–4510 (2010).
[74]T. Lu, C. Keplinger, N. Arnold, S. Bauer, and Z. Suo, "Charge localization instability in a highly deformable dielectric elastomer," Appl. Phys. Lett. **104**, 022905 (2014).
[75]B. Li, J. Zhou, and H. Chen, "Electromechanical stability in charge-controlled dielectric elastomer actuation," Appl. Phys. Lett. **99**, 244101 (2011).
[76]X. H. Zhao and Z. G. Suo, "Method to analyze programmable deformation of dielectric elastomer layers," Appl. Phys. Lett. **93**, 251902 (2008).
[77]M. Watanabe, H. Shirai, and T. Hirai, "Wrinkled polypyrrole electrode for electroactive polymer actuators," J. Appl. Phys. **92**, 4631–4637 (2002).
[78]S. Rosset and H. R. Shea, "Flexible and stretchable electrodes for dielectric elastomer actuators," Appl. Phys. A: Mater. Sci. Process. **110**, 281–307 (2013).
[79]M. R. Begley, H. Bart-Smith, O. N. Scott, M. H. Jones, and M. L. Reed, "The electro-mechanical response of elastomer membranes coated with ultra-thin metal electrodes," J. Mech. Phys. Solids **53**, 2557–2578 (2005).

[80]W. Yuan *et al.*, "Fault-tolerant dielectric elastomer actuators using single-walled carbon nanotube electrodes," Adv. Mater. **20**, 621 (2008).
[81]D. J. Lipomi *et al.*, "Skin-like pressure and strain sensors based on transparent elastic films of carbon nanotubes," Nat. Nanotechnol. **6**, 788–792 (2011).
[82]Y. Zhu and F. Xu, "Buckling of aligned carbon nanotubes as stretchable conductors: A new manufacturing strategy," Adv. Mater. **24**, 1073–1077 (2012).
[83]H. Stoyanov *et al.*, "Long lifetime, fault-tolerant freestanding actuators based on a silicone dielectric elastomer and self-clearing carbon nanotube compliant electrodes," RSC Adv. **3**, 2272–2278 (2013).
[84]F. Xu and Y. Zhu, "Highly conductive and stretchable silver nanowire conductors," Adv. Mater. **24**, 5117–5122 (2012).
[85]J. H. Wu, J. F. Zang, A. R. Rathmell, X. H. Zhao, and B. J. Wiley, "Reversible sliding in networks of nanowires," Nano Lett. **13**, 2381–2386 (2013).
[86]S. Yun *et al.*, "Compliant silver nanowire-polymer composite electrodes for bistable large strain actuation," Adv. Mater. **24**, 1321–1327 (2012).
[87]S. Zhu *et al.*, "Ultrastretchable fibers with metallic conductivity using a liquid metal alloy core," Adv. Funct. Mater. **23**, 2308–2314 (2013).
[88]C. Keplinger *et al.*, "Stretchable, transparent, ionic conductors," Science **341**, 984–987 (2013).
[89]J. A. Rogers, "A clear advance in soft actuators," Science **341**, 968–969 (2013).
[90]B. Chu *et al.*, "A dielectric polymer with high electric energy density and fast discharge speed," Science **313**, 334–336 (2006).
[91]J. S. Plante and S. Dubowsky, "Large-scale failure modes of dielectric elastomer actuators," Int. J. Solids Struct. **43**, 7727–7751 (2006).
[92]W. G. Lawson, "Temperature dependence of intrinsic electric strength of polythene," Nature **206**, 1248 (1965).
[93]J. Blok and D. G. LeGrand, "Dielectric breakdown of polymer films," J. Appl. Phys. **40**, 288 (1969).
[94]D. B. Watson, "Dielectric breakdown in perspex," IEEE Trans. Electr. Insul. **EI-8**, 73–75 (1973).
[95]M. Ieda, "Dielectric-breakdown process of polymers," IEEE Trans. Electr. Insul. **EI-15**, 206–224 (1980).
[96]N. Yoshimura, M. Nishida, and F. Noto, "Dielectric-breakdown of polyethersulfone (PES) film under DC voltage conditions," IEEE Trans. Electr. Insul. **EI-17**, 359–362 (1982).
[97]H. R. Zeller and W. R. Schneider, "Electrofracture mechanics of dielectric aging," J. Appl. Phys. **56**, 455 (1984).
[98]P. Guerin *et al.*, "Pressure and temperature-dependence of the dielectric-breakdown of polyethylene used in submarine power-cables," J. Appl. Phys. **57**, 4805–4807 (1985).
[99]M. Hikita *et al.*, "High-field conduction and electrical breakdown of polyethylene at high-temperatures," Jpn. J. Appl. Phys. Part 1 **24**, 988–996 (1985).
[100]M. Farkh *et al.*, "Dielectric-breakdown of high-density polyethylene (HDPE) under high-pressure," J. Phys. D: Appl. Phys. **22**, 566–568 (1989).
[101]J. C. Fothergill, "Filamentary electromechanical breakdown," IEEE Trans. Electr. Insul. **26**, 1124 (1991).
[102]N. Zebouchi, R. Essolbi, D. Malec, H. T. Giam, and B. Ai, "Electrical breakdown of polyethylene terephthalate under hydrostatic-pressure," J. Appl. Phys. **76**, 8218–8220 (1994).
[103]A. Tröls *et al.*, "Stretch dependence of the electrical breakdown strength and dielectric constant of dielectric elastomers," Smart Mater. Struct. **22**, 104012 (2013).
[104]C. Keplinger, M. Kaltenbrunner, N. Arnold, and S. Bauer, "Capacitive extensometry for transient strain analysis of dielectric elastomer actuators," Appl. Phys. Lett. **92**, 192903 (2008).
[105]J. Zhu, M. Kollosche, T. Lu, G. Kofod, and Z. Suo, "Two types of transitions to wrinkles in dielectric elastomers," Soft Matter **8**, 8840–8846 (2012).
[106]Y. Liu, L. Liu, Z. Zhang, L. Shi, and J. Leng, "Comment on 'method to analyze electromechanical stability of dielectric elastomers' [Appl. Phys. Lett. 91, 061921 (2007)]," Appl. Phys. Lett. **93**, 106101 (2008).
[107]A. N. Norris, "Comment on 'Method to analyze electromechanical stability of dielectric elastomers' [Appl. Phys. Lett. 91, 061921 (2007)]," Appl. Phys. Lett. **92**, 026101 (2008).
[108]M. Wissler and E. Mazza, "Modeling and simulation of dielectric elastomer actuators," Smart Mater. Struct. **14**, 1396–1402 (2005).
[109]M. Wissler and E. Mazza, "Electromechanical coupling in dielectric elastomer actuators," Sens. Actuators A: Phys. **138**, 384–393 (2007).
[110]M. Wissler and E. Mazza, "Mechanical behavior of an acrylic elastomer used in dielectric elastomer actuators," Sens. Actuators A: Phys. **134**, 494–504 (2007).
[111]N. Goulbourne, E. Mockensturm, and M. Frecker, "A nonlinear model for dielectric elastomer membranes," J. Appl. Mech. **72**, 899 (2005).
[112]N. C. Goulbourne, E. M. Mockensturm, and M. I. Frecker, "Electro-elastomers: Large deformation analysis of silicone membranes," Int. J. Solids Struct. **44**, 2609–2626 (2007).
[113]J. S. Leng, L. W. Liu, Y. J. Liu, K. Yu, and S. H. Sun, "Electromechanical stability of dielectric elastomer," Appl. Phys. Lett. **94**, 211901 (2009).
[114]B. Li *et al.*, "Effect of mechanical pre-stretch on the stabilization of dielectric elastomer actuation," J. Phys. D: Appl. Phys. **44**, 155301 (2011).
[115]R. Diaz-Calleja, M. J. Sanchis, and E. Riande, "Effect of an electric field on the bifurcation of a biaxially stretched incompressible slab rubber," Eur. Phys. J. E **30**, 417–426 (2009).
[116]X. H. Zhao, W. Hong, and Z. G. Suo, "Stretching and polarizing a dielectric gel immersed in a solvent," Int. J. Solids Struct. **45**, 4021–4031 (2008).
[117]E. Hohlfeld and L. Mahadevan, "Unfolding the sulcus," Phys. Rev. Lett. **106**, 105702 (2011).
[118]Q. Wang and X. Zhao, "Phase diagrams of instabilities in compressed film-substrate systems," J. Appl. Mech. **81**, 051004 (2014).
[119]W. Hong, X. H. Zhao, and Z. G. Suo, "Formation of creases on the surfaces of elastomers and gels," Appl. Phys. Lett. **95**, 111901 (2009).
[120]V. Shenoy and A. Sharma, "Pattern formation in a thin solid film with interactions," Phys. Rev. Lett. **86**, 119–122 (2001).
[121]R. Huang, "Electrically induced surface instability of a conductive thin film on a dielectric substrate," Appl. Phys. Lett. **87**, 151911 (2005).
[122]L. F. Pease and W. B. Russel, "Linear stability analysis of thin leaky dielectric films subjected to electric fields," J. Non-Newtonian Fluid Mech. **102**, 233–250 (2002).
[123]Q. M. Wang and X. H. Zhao, "Creasing-wrinkling transition in elastomer films under electric fields," Phys. Rev. E **88**, 042403 (2013).
[124]M. Biot, "Surface instability of rubber in compression," Appl. Sci. Res., Sect. A **12**, 168–182 (1963).
[125]Y. P. Cao and J. W. Hutchinson, "From wrinkles to creases in elastomers: The instability and imperfection-sensitivity of wrinkling," Proc. R. Soc. A: Math. Phys. Eng. Sci. **468**, 94–115 (2012).
[126]W. H. Wong, T. F. Guo, Y. W. Zhang, and L. Cheng, "Surface instability maps for soft materials," Soft Matter **6**, 5743–5750 (2010).
[127]H. S. Park, Q. M. Wang, X. H. Zhao, and P. A. Klein, "Electromechanical instability on dielectric polymer surface: Modeling and experiment," Comput. Methods Appl. Mech. Eng. **260**, 40–49 (2013).
[128]H. S. Park and T. D. Nguyen, "Viscoelastic effects on electromechanical instabilities in dielectric elastomers," Soft Matter **9**, 1031–1042 (2013).
[129]G. Finis and A. Claudi, "On the electric breakdown behavior of Silicone gel at interfaces," IEEE Trans. Dielectr. Electr. Insul. **15**, 366–373 (2008).
[130]J. A. Stratton, *Electromagnetic Theory* (Wiley-IEEE Press, 2007), Vol. 33.
[131]G. Taylor, "Disintegration of water drops in electric field," Proc. R. Soc. London, Ser. A **280**, 383 (1964).
[132]L. D. Landau *et al.*, *Electrodynamics of Continuous Media* (Pergamon Press, Oxford, 1960), Vol. 364.
[133]P. J. Flory, *Principles of Polymer Chemistry* (Cornell University Press, 1953).
[134]M. Rubinstein and R. H. Colby, *Polymer Physics* (Oxford University Press, 2003).
[135]L. R. G. Treloar, *The Physics of Rubber Elasticity* (Clarendon Press, 1975).
[136]M. C. Boyce and E. M. Arruda, "Constitutive models of rubber elasticity: A review," Rubber Chem. Technol. **73**, 504 (2000).
[137]S. J. A. Koh *et al.*, "Mechanisms of large actuation strain in dielectric elastomers," J. Polym. Sci., Part B: Polym. Phys. **49**, 504–515 (2011).
[138]Z. G. Suo and J. Zhu, "Dielectric elastomers of interpenetrating networks," Appl. Phys. Lett. **95**, 232909 (2009).
[139]S. M. Ha, W. Yuan, Q. B. Pei, R. Pelrine, and S. Stanford, "Interpenetrating polymer networks for high-performance electroelastomer artificial muscles," Adv. Mater. **18**, 887–891 (2006).
[140]R. Shankar, T. K. Ghosh, and R. J. Spontak, "Electromechanical response of nanostructured polymer systems with no mechanical pre-strain," Macromol. Rapid Commun. **28**, 1142–1147 (2007).

[141]S. M. Ha, W. Yuan, Q. Pei, R. Pelrine, and S. Stanford, "Interpenetrating networks of elastomers exhibiting 300% electrically-induced area strain," Smart Mater. Struct. **16**, S280–S287 (2007).
[142]X. F. Niu *et al*., "Synthesizing a new dielectric elastomer exhibiting large actuation strain and suppressed electromechanical instability without pre-stretching," J. Polym. Sci. Part B: Polym. Phys. **51**, 197–206, (2013).
[143]Y. Jang, T. Hirai, T. Ueki, and T. Kato, "Enhancement of the actuation performance of dielectric triblock copolymers modified with additives," Polym. Int. **61**, 228–234 (2012).
[144]G. Kofod, "The static actuation of dielectric elastomer actuators: How does pre-stretch improve actuation?" J. Phys. D: Appl. Phys. **41**, 215405 (2008).
[145]M. Wissler and E. Mazza, "Modeling of a pre-strained circular actuator made of dielectric elastomers," Sens. Actuators A: Phys. **120**, 184–192 (2005).
[146]Q. Pei, R. Pelrine, S. Stanford, R. Kornbluh, and M. Rosenthal, "Electroelastomer rolls and their application for biomimetic walking robots," Synth. Met. **135–136**, 129–131 (2003).
[147]S. Rudykh, K. Bhattacharya, and G. deBotton, "Snap-through actuation of thick-wall electroactive balloons," Int. J. Non-Linear Mech. **47**, 206–209 (2012).
[148]J. Zhu, S. Cai, and Z. Suo, "Nonlinear oscillation of a dielectric elastomer balloon," Polym. Int. **59**, 378–383 (2010).
[149]F. Carpi, C. Salaris, and D. De Rossi, "Folded dielectric elastomer actuators," Smart Mater. Struct. **16**, S300–S305 (2007).
[150]F. Carpi, A. Migliore, G. Serra, and D. De Rossi, "Helical dielectric elastomer actuators," Smart Mater. Struct. **14**, 1210–1216 (2005).
[151]T. H. He, X. H. Zhao, and Z. G. Suo, "Dielectric elastomer membranes undergoing inhomogeneous deformation," J. Appl. Phys. **106**, 083522 (2009).
[152]G. Berselli, R. Vertechy, G. Vassura, and V. Parenti-Castelli, "Optimal synthesis of conically shaped dielectric elastomer linear actuators: Design methodology and experimental validation," IEEE-ASME Trans. Mechatron. **16**, 67–79 (2011).
[153]S. Arora, T. Ghosh, and J. Muth, "Dielectric elastomer based prototype fiber actuators," Sens. Actuators A: Phys. **136**, 321–328 (2007).
[154]A. Wingert, M. D. Lichter, and S. Dubowsky, "On the design of large degree-of-freedom digital mechatronic devices based on bistable dielectric elastomer actuators," IEEE-ASME Trans. Mechatron. **11**, 448–456 (2006).
[155]J. Fothergil, L. Dissado, and P. Sweeney, "A discharge-avalanche theory for the propagation of electrical tree: a physical basis for their voltage," IEEE Trans. Dielectr. Electr. Insul. **1**, 474–486 (1994).
[156]C. Mayoux, "Degradation of insulating materials under electrical stress," IEEE Trans. Dielectr. Electr. Insul. **7**, 590–601 (2000).
[157]M. Kollosche and G. Kofod, "Electrical failure in blends of chemically identical, soft thermoplastic elastomers with different elastic stiffness," Appl. Phys. Lett. **96**, 071904 (2010).
[158]R. Huang and Z. G. Suo, "Electromechanical phase transition in dielectric elastomers," Proc. R. Soc. A: Math. Phys. Eng. Sci. **468**, 1014–1040 (2012).
[159]T. Li *et al*., "Giant voltage-induced deformation in dielectric elastomers near the verge of snap-through instability," J. Mech. Phys. Solids **61**, 611–628 (2013).
[160]T. L. Sun *et al*., "Reversible switching between superhydrophilicity and superhydrophobicity," Angew. Chem., Int. Ed. **43**, 357–360 (2004).
[161]H. J. Gao and H. M. Yao, "Shape insensitive optimal adhesion of nanoscale fibrillar structures," Proc. Natl. Acad. Sci. U. S. A. **101**, 7851–7856 (2004).
[162]E. P. Chan, E. J. Smith, R. C. Hayward, and A. J. Crosby, "Surface wrinkles for smart adhesion," Adv. Mater. **20**, 711–716 (2008).
[163]J. L. Wilbur *et al*., "Elastomeric optics," Chem. Mater. **8**, 1380–1385 (1996).
[164]X. H. Zhao *et al*., "Active scaffolds for on-demand drug and cell delivery," Proc. Natl. Acad. Sci. U. S. A. **108**, 67–72 (2011).
[165]L. K. Ista, S. Mendez, and G. P. Lopez, "Attachment and detachment of bacteria on surfaces with tunable and switchable wettability," Biofouling **26**, 111–118 (2010).
[166]M. A. Meitl *et al*., "Transfer printing by kinetic control of adhesion to an elastomeric stamp," Nature Mater. **5**, 33–38 (2006).
[167]L. Hall-Stoodley, J. W. Costerton, and P. Stoodley, "Bacterial biofilms: From the natural environment to infectious diseases," Nat. Rev. Microbiol. **2**, 95–108 (2004).
[168]D. M. Yebra, S. Kiil, and K. Dam-Johansen, "Antifouling technology—Past, present and future steps towards efficient and environmentally friendly antifouling coatings," Prog. Org. Coat. **50**, 75–104 (2004).
[169]J. A. Callow and M. E. Callow, "Trends in the development of environmentally friendly fouling-resistant marine coatings," Nat. Commun. **2**, 244 (2011).
[170]E. Ralston and G. Swain, "Bioinspiration—The solution for biofouling control?" Bioinspiration Biomimetics **4**, 015007 (2009).
[171]A. Wanner, "Clinical aspects of mucociliary transport," Am. Rev. Respir. Dis. **116**, 73–125 (1977).
[172]H. Matsui *et al*., "Evidence for periciliary liquid layer depletion, not abnormal ion composition, in the pathogenesis of cystic fibrosis airways disease," Cell **95**, 1005–1015 (1998).
[173]T. Sanchez, D. Welch, D. Nicastro, and Z. Dogic, "Cilia-like beating of active microtubule bundles," Science **333**, 456–459 (2011).
[174]M. Wahl, K. Kroger, and M. Lenz, "Non-toxic protection against epibiosis," Biofouling **12**, 205–226 (1998).
[175]S. Bauer *et al*., "25th Anniversary article: A soft future from robots and sensor skin to energy harvesters," Adv. Mater. **26**, 149–162 (2014).
[176]N. Lu and D.-H. Kim, "Flexible and stretchable electronics paving the way for soft robotics," Soft Rob. **1**, 53–62 (2014).
[177]J. A. Rogers, T. Someya, and Y. Huang, "Materials and mechanics for stretchable electronics," Science **327**, 1603–1607 (2010).
[178]J. D. Madden, "Mobile robots: Motor challenges and materials solutions," Science **318**, 1094–1097 (2007).
[179]Z. G. Suo, in *Mechanics of Stretchable Electronics and Soft Machines*, edited by S. Wagner and S. Bauer (Mater. Res. Sci. Bull., 2012), Vol. 37, pp. 218–225.
[180]T. Yamwong, A. M. Voice, and G. R. Davies, "Electrostrictive response of an ideal polar rubber," J. Appl. Phys. **91**, 1472–1476 (2002).
[181]G. Kofod, P. Sommer-Larsen, R. Kornbluh, and R. Pelrine, "Actuation response of polyacrylate dielectric elastomers," J. Intell. Mater. Syst. Struct. **14**, 787–793 (2003).
[182]L. W. Liu, Y. J. Liu, X. J. Luo, B. Li, and J. S. Leng, "Electromechanical instability and snap-through instability of dielectric elastomers undergoing polarization saturation," Mech. Mater. **55**, 60–72 (2012).
[183]Y. M. Shkel and D. Klingenberg, "Material parameters for electrostriction," J. Appl. Phys. **80**, 4566–4572 (1996).
[184]X. H. Zhao and Z. G. Suo, "Electrostriction in elastic dielectrics undergoing large deformation," J. Appl. Phys. **104**, 123530 (2008).
[185]S. M. A. Jimenez and R. M. McMeeking, "Deformation dependent dielectric permittivity and its effect on actuator performance and stability," Int. J. Non-Linear Mech. **57**, 183–191 (2013).
[186]W. Ma and L. E. Cross, "An experimental investigation of electromechanical response in a dielectric acrylic elastomer," Appl. Phys. A: Mater. Sci. Process. **78**, 1201–1204 (2004).
[187]B. Li, L. Liu, and Z. Suo, "Extension limit, polarization saturation, and snap-through instability of dielectric elastomers," Int. J. Smart Nano Mater. **2**, 59–67 (2011).
[188]B. Li, H. L. Chen, J. X. Zhou, Z. C. Zhu, and Y. Q. Wang, "Polarization-modified instability and actuation transition of deformable dielectric," EPL **95**, 37006 (2011).
[189]C. C. Foo, S. Cai, S. J. A. Koh, S. Bauer, and Z. Suo, "Model of dissipative dielectric elastomers," J. Appl. Phys. **111**, 034102 (2012).
[190]J.-S. Plante and S. Dubowsky, "On the performance mechanisms of dielectric elastomer actuators," Sens. Actuators A: Phys. **137**, 96–109 (2007).
[191]W. Hong, "Modeling viscoelastic dielectrics," J. Mech. Phys. Solids **59**, 637–650 (2011).
[192]Y. Bai, Y. Jiang, B. Chen, C. C. Foo, Y. Zhou, F. Xiang, J. Zhou, H. Wang, and Z. Suo, "Cyclic performance of viscoelastic dielectric elastomers with solid hydrogel electrodes," Appl. Phys. Lett. **104**, 062902 (2014).
[193]X. H. Zhao, S. J. A. Koh, and Z. G. Suo, "Nonequilibrium thermodynamics of dielectric elastomers," Int. J. Appl. Mech. **3**, 203–217 (2011).
[194]H. Wang, M. Lei, and S. Cai, "Viscoelastic deformation of a dielectric elastomer membrane subject to electromechanical loads," J. Appl. Phys. **113**, 213508 (2013).
[195]P. Lochmatter, G. Kovacs, and M. Wissler, "Characterization of dielectric elastomer actuators based on a visco-hyperelastic film model," Smart Mater. Struct. **16**, 477–486 (2007).
[196]T. F. Li, S. X. Qu, and W. Yang, "Energy harvesting of dielectric elastomer generators concerning inhomogeneous fields and viscoelastic deformation," J. Appl. Phys. **112**, 034119 (2012).
[197]H. Gao, T.-Y. Zhang, and P. Tong, "Local and global energy release rates for an electrically yielded crack in a piezoelectric ceramic," J. Mech. Phys. Solids **45**, 491–510 (1997).

[198]X. H. Zhao, "A theory for large deformation and damage of interpenetrating polymer networks," J. Mech. Phys. Solids **60**, 319–332 (2012).
[199]Q. Liu, D. Guyomar, L. Seveyrat, and B. Guiffard, "A study on a polyurethane-based blend with enhanced electromechanical properties," J. Optoelectron. Adv. Mater. **15**, 475–480 (2013).
[200]G. Gallone, F. Galantini, and F. Carpi, "Perspectives for new dielectric elastomers with improved electromechanical actuation performance: Composites versus blends," Polym. Int. **59**, 400–406 (2010).
[201]C. Huang, Q. M. Zhang, and J. Su, "High-dielectric-constant all-polymer percolative composites," Appl. Phys. Lett. **82**, 3502–3504 (2003).
[202]F. Carpi, G. Gallone, F. Galantini, and D. De Rossi, "Silicone-poly(hexylthiophene) blends as elastomers with enhanced electromechanical transduction properties," Adv. Funct. Mater. **18**, 235–241 (2008).
[203]B. Kussmaul *et al.*, "Enhancement of dielectric permittivity and electromechanical response in silicone elastomers: Molecular grafting of organic dipoles to the macromolecular network," Adv. Funct. Mater. **21**, 4589–4594 (2011).
[204]Y. G. Wu, X. H. Zhao, F. Li, and Z. G. Fan, "Evaluation of mixing rules for dielectric constants of composite dielectrics by MC-FEM calculation on 3D cubic lattice," J. Electroceram. **11**, 227–239 (2003).
[205]X. H. Zhao, Y. G. Wu, Z. G. Fan, and F. Li, "Three-dimensional simulations of the complex dielectric properties of random composites by finite element method," J. Appl. Phys. **95**, 8110–8117 (2004).
[206]F. Carpi and D. De Rossi, "Improvement of electromechanical actuating performances of a silicone dielectric elastomer by dispersion of titanium dioxide powder," IEEE Trans. Dielectr. Electr. Insul. **12**, 835–843 (2005).
[207]G. Gallone, F. Carpi, D. De Rossi, G. Levita, and A. Marchetti, "Dielectric constant enhancement in a silicone elastomer filled with lead magnesium niobate-lead titanate," Mater. Sci. Eng. C: Biomimetic Supramol. Syst. **27**, 110–116 (2007).
[208]O. Lopez-Pamies, "Elastic dielectric composites: Theory and application to particle-filled ideal dielectrics," J. Mech. Phys. Solids **64**, 61 (2014).
[209]P. P. Castaneda and M. N. Siboni, "A finite-strain constitutive theory for electro-active polymer composites via homogenization," Int. J. Non-Linear Mech. **47**, 293–306 (2012).
[210]M. Molberg *et al.*, "High breakdown field dielectric elastomer actuators using encapsulated polyaniline as high dielectric constant filler," Adv. Funct. Mater. **20**, 3280–3291 (2010).
[211]H. Stoyanov, M. Kollosche, S. Risse, D. N. McCarthy, and G. Kofod, "Elastic block copolymer nanocomposites with controlled interfacial interactions for artificial muscles with direct voltage control," Soft Matter **7**, 194–202 (2011).
[212]D. M. Opris *et al.*, "New silicone composites for dielectric elastomer actuator applications in competition with acrylic foil," Adv. Funct. Mater. **21**, 3531–3539 (2011).
[213]D. N. McCarthy *et al.*, "Increased permittivity nanocomposite dielectrics by controlled interfacial interactions," Compos. Sci. Technol. **72**, 731–736 (2012).
[214]W. Y. Li and C. M. Landis, "Deformation and instabilities in dielectric elastomer composites," Smart Mater. Struct. **21**, 094006 (2012).
[215]K. Bertoldi and M. Gei, "Instabilities in multilayered soft dielectrics," J. Mech. Phys. Solids **59**, 18–42 (2011).
[216]M. Gei, R. Springhetti, and E. Bortot, "Performance of soft dielectric laminated composites," Smart Mater. Struct. **22**, 104014 (2013).
[217]C. Y. Cao and X. H. Zhao, "Tunable stiffness of electrorheological elastomers by designing mesostructures," Appl. Phys. Lett. **103**, 041901 (2013).
[218]S. Rudykh, A. Lewinstein, G. Uner, and G. deBotton, "Analysis of microstructural induced enhancement of electromechanical coupling in soft dielectrics," Appl. Phys. Lett. **102**, 151905 (2013).
[219]L. Tian, L. Tevet-Deree, G. deBotton, and K. Bhattacharya, "Dielectric elastomer composites," J. Mech. Phys. Solids **60**, 181–198 (2012).
[220]G. Shmuel and G. deBotton, "Band-gaps in electrostatically controlled dielectric laminates subjected to incremental shear motions," J. Mech. Phys. Solids **60**, 1970–1981 (2012).
[221]S. A. Spinelli and O. Lopez-Pamies, "Some simple explicit results for the elastic dielectric properties and stability of layered composites," Int. J. Eng. Sci. (published online).
[222]T. Lu *et al.*, "Dielectric elastomer actuators under equal-biaxial forces, uniaxial forces, and uniaxial constraint of stiff fibers," Soft Matter **8**, 6167–6173 (2012).
[223]G. Shmuel, "Electrostatically tunable band gaps in finitely extensible dielectric elastomer fiber composites," Int. J. Solids Struct. **50**, 680–686 (2013).
[224]J. Huang, T. Lu, J. Zhu, D. R. Clarke, and Z. Suo, "Large, uni-directional actuation in dielectric elastomers achieved by fiber stiffening," Appl. Phys. Lett. **100**, 041911 (2012).
[225]B. O'Brien, T. McKay, E. Calius, S. Xie, and I. Anderson, "Finite element modelling of dielectric elastomer minimum energy structures," Appl. Phys. A: Mater. Sci. Process. **94**, 507–514 (2009).
[226]J. X. Zhou, W. Hong, X. H. Zhao, Z. Q. Zhang, and Z. G. Suo, "Propagation of instability in dielectric elastomers," Int. J. Solids Struct. **45**, 3739–3750 (2008).
[227]D. K. Vu, P. Steinmann, and G. Possart, "Numerical modelling of non-linear electroelasticity," Int. J. Numer. Methods Eng. **70**, 685–704 (2007).
[228]D. L. Henann, S. A. Chester, and K. Bertoldi, "Modeling of dielectric elastomers: Design of actuators and energy harvesting devices," J. Mech. and Phys. Solids **61**, 2047–2066 (2013).
[229]R. M. McMeeking, C. M. Landis, and S. M. A. Jimenez, "A principle of virtual work for combined electrostatic and mechanical loading of materials," Int. J. Non-Linear Mech. **42**, 831–838 (2007).
[230]S. X. Qu and Z. G. Suo, "A finite element method for dielectric elastomer transducers," Acta Mech. Solida Sin. **25**, 459–466 (2012).
[231]K. A. Khan, H. Wafai, and T. El Sayed, "A variational constitutive framework for the nonlinear viscoelastic response of a dielectric elastomer," Comput. Mech. **52**, 345–360 (2013).
[232]J. W. Fox and N. C. Goulbourne, "On the dynamic electromechanical loading of dielectric elastomer membranes," J. Mech. Phys. Solids **56**, 2669–2686 (2008).
[233]J. A. Zhu, S. Q. Cai, and Z. G. Suo, "Resonant behavior of a membrane of a dielectric elastomer," Int. J. Solids Struct. **47**, 3254–3262 (2010).
[234]J. W. Fox and N. C. Goulbourne, "Electric field-induced surface transformations and experimental dynamic characteristics of dielectric elastomer membranes," J. Mech. Phys. Solids **57**, 1417–1435 (2009).
[235]P. B. Goncalves, R. M. Soares, and D. Pamplona, "Nonlinear vibrations of a radially stretched circular hyperelastic membrane," J. Sound Vib. **327**, 231–248 (2009).
[236]H. S. Park, Z. G. Suo, J. X. Zhou, and P. A. Klein, "A dynamic finite element method for inhomogeneous deformation and electromechanical instability of dielectric elastomer transducers," Int. J. Solids Struct. **49**, 2187–2194 (2012).